INTEGRATION OF ACTIVE CONTROL AND PASSIVE COMPLIANCE FOR PEG-AND-HOLE ASSEMBLY

A Thesis

Submitted to the Faculty

of

Purdue University

by

Yuerong Li

In Partial Fulfillment of the

Requirements for the Degree

of

Master of Science

Dec 2020

Purdue University

West Lafayette, Indiana

THE PURDUE UNIVERSITY GRADUATE SCHOOL
STATEMENT OF THESIS APPROVAL

Dr. Bin Yao, Chair

School of Mechanical Engineering

Dr. Peter H. Meckl

School of Mechanical Engineering

Dr. Martin J. Corless

School of Aeronautics and Astronautics

Approved by:

Dr. Nicole L. Key

Head of the School Graduate Program

TABLE OF CONTENTS

Page

LIST OF FIGURES

SYMBOLS

r	The peg radius
R	The hole radius
$\vec{r}_{cc}$	The compliance center in the peg coordinate
r_{ccx}	The x component of $\vec{r}_{cc}$
r_{ccz}	The z component of $\vec{r}_{cc}$
θ_y	The error angle between the peg and the hole
ϵ_x	The horizontal error between the peg and the hole
K_x	The lateral stiffness of the compliance matrix
K_{R_y}	The torsion stiffness of the compliance matrix
D_x	The x component of compliance center location in the hole coordinate
T_x	Additional position control input along x axis
R_y	Additional angle control input about y axis
α	The chamfer angle
μ	The friction coefficient between the peg and the hole
s	The distance to the hole along chamfer
l	The inserted depth

ABBREVIATIONS

RCC	Remote Compliance Center
VRCC	Variable Remote Compliance Center

ABSTRACT

Li, Yuerong MS, Purdue University, Dec 2020. Integration of Active Control and Passive Compliance for Peg-and-Hole Assembly. Major Professor: Bin Yao, School of Mechanical Engineering.

This thesis provides a brief intro to the peg-and-hole problem and goes through two active and passive compliance strategies as well as the cases that the compliance center position is not ideal. A specific scenario of peg being gripped at an error angle due to large vision uncertainties is raised and studied. Such setup can lead to an off compliance center position relative to the peg and can happen in real life but has not been solved by previous approaches. A potential solution to it by combining active control and passive compliance is provided and analyzed. By using the force and torque feedback and the robot joint angle information, the compliance center for the above scenario could be estimated without vision feedback to by-pass the potential accuracy limitation of vision sensors. And a position control with reference determined in real-time by these sensors would be able to cancel out the majority of the effect caused by an off compliance center. Additional recommendations to future work on integration of active and passive compliance strategies and utilization of arbitrary compliance center positions are provided as well.

1. INTRODUCTION

This chapter will first talk about why the peg-and-hole problem is worth studying and discuss how some other researchers have approached the problem. It then compares the pros and cons of commonly used passive compliance and active compliance assembly strategies. After that, the purpose and motivation behind this thesis are explained. Lastly, an assumption to simplify the analysis is brought out, but the resulting problem is still difficult to solve. Chapter 2 will go over some traditional peg-and-hole problem analyses. The peg-and-hole problem with off compliance center as well as the potential solution to it are discussed in chapter 3. Quantitative analysis and simulation results are presented in chapter 4. Finally, chapter 5 concludes the thesis and chapter 6 gives recommendations for future work.

1.1 Peg-and-hole Problem

Peg-and-hole assembly problems have been widely studied over the last 70 years as they represent tasks that are commonly required in industry and daily life and yet difficult to perform by industrial robots. The non-linearity of reaction forces during different contact states based on the geometry and orientation and position freedom of the peg and the hole made the problem require certain devices and control strategies to avoid jamming. In the meantime, with the rapid advancement in robotics, more and more repetitive assembly tasks in industrial factories have been done by robotic arms, including from putting tiny capacitors on electronics boards to mounting vehicle bodies to chassis. Nowadays even more complicated real life services provided by robots contain assembly problems, such as plugging in charging cables.

Most commonly seen strategies for a peg-and-hole problem can be divided into the group focusing on using a passive compliance device and the one focusing on using

active controls. The Remote Compliance Center [1], introduced by Whitney and his colleagues in reference [2] around 1980s, is a passive compliance device that places the compliance center near the end of the peg to help avoid jamming. Later on there are also papers about designing and analyzing practical passive compliance devices based on material deformation such as reference [3] and square peg-and-hole problem using a passive compliance device [4]. On the other hand, more research has been done around active compliance force control due to the fast progress of chip calculation ability, sensor accuracy and machine learning models. The active control can be further divided into model based and model free [5]. Model free assembly utilizes a general force control strategy throughout the process, which is commonly seen in early works [6], multi-peg problems when contact states are complicated [7], and new learning approaches like reference [8]. And model based strategies consist of categorization into contact states from sensor information and active control algorithms in each specific state [9] [10]. There are also many additional papers related to the peg-and-hole problem that did not focus on the inserting phase, but on other aspects such as how to locate the hole by active searching using various approaches [11] or by analyzing force and torque sensor results [12].

1.2 Active versus Passive Compliance

Although there is already so much research in this area, how active control and passive compliance device approaches can be combined is less studied. Reference [13] provides a detailed comparison between the two. The pros and cons can be summarized as follows.

The biggest advantage of passive compliance devices is that they can overcome the lack of accuracy and dexterity of the actuators. So the cost is usually lower due to the lower requirement of the control unit. Also the response speed and reliability of a working passive compliance device is usually much better. However, general passive

compliance devices require specific design for each case and cannot adjust when the initial error is really large.

Active compliance, on the other hand, can have dynamic compliance configuration and move the compliance center easily. So simply changing some parameter values might allow active compliance to be used on a whole different setup. And active compliance can deal with large errors when paying additional attention to those cases. But active compliance also suffers from singularity, dexterity and accuracy limits of the robot arms and response speed limits of the control loop.

1.3 Arbitrary Compliance Center

It is also noticed that for most compliance strategy analysis, the compliance center is assumed to be sitting on the middle line of the peg. However, if the peg is picked up by a robot arm instead of mounted on it, especially when vision is used to locate the item in a complicated environment, uncertainties can lead to the actual compliance center relative to the peg not at the ideal position. And to utilize the advantages from both active and passive compliance, it would be expected that the same passive compliance device needs to be used on various peg-and-hole assemblies. Since the compliance center from passive devices needs to be designed beforehand, even with the Variable Remote Compliance Center [14], the pegs would probably encounter cases in which the compliance center is not at the tip of the peg as planned. And no matter how the peg is connected to the robot, in the real world, compliance exists. Therefore, studying the effect that an arbitrary compliance center has on the peg-and-hole assembly problem is meaningful. Also it would be shown later how potential integration of active control and passive compliance strategy could be used to have an arbitrary compliance center case behave as if the compliance center is ideal.

1.4 Simplified 2-D Peg-and-hole Problem

Peg-and-hole problem is about robots mating two parts together. The part being inserted, the peg, is usually a small long object while the other part, the hole, is a bigger piece containing a concave space that has a similar cross section shape as the peg. Sometimes a chamfer, a tilted surface around the hole entrance, is present to help guide the peg into the hole. Some unusual shape peg-and-hole problems [15], multi-pin peg-and-hole problems [16] and chamferless peg-and-hole problems [17] also see a lot of research. But the simplest case would be a perfect cylinder shape peg and a straight round hole with chamfer. Due to the symmetric property of this design, the problem can then be simplified to be set in a 2-D scenario. Thus the degrees of freedom would be smaller, the contact cases would be fewer and the equations would be more straightforward to analyze to reach certain conclusions. And just like many other papers, this thesis assumes only two degrees of translation and one degree of rotation freedom in 2-D.

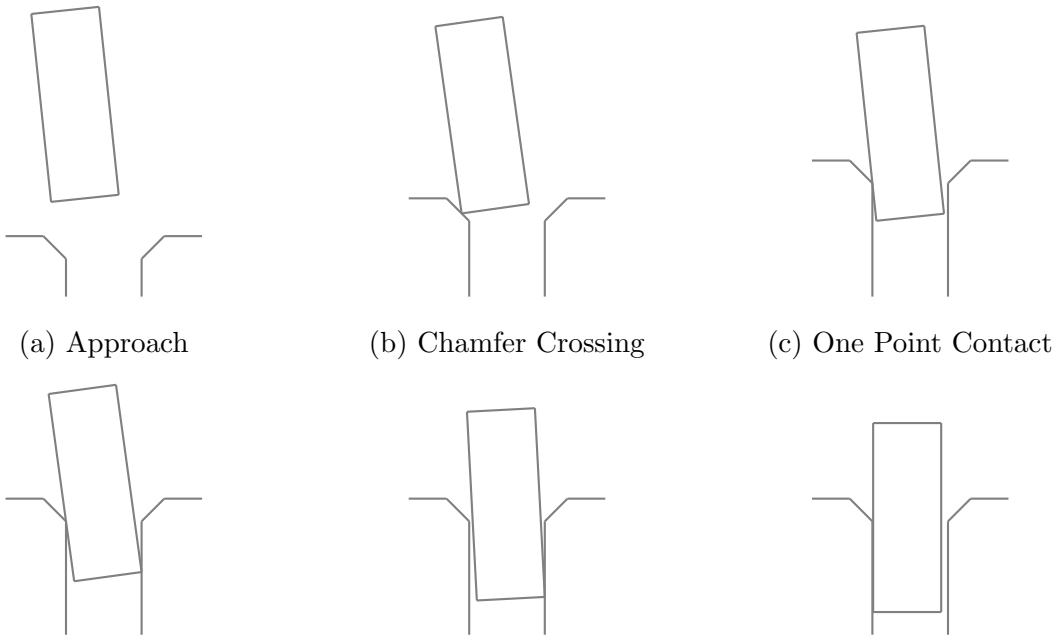

(a) Approach (b) Chamfer Crossing (c) One Point Contact

(d) Two Point Contact (e) One Point Contact (f) Surface Contact

Figure 1.1. : The Contact States for Peg-and-hole Problems in 2-D

A full peg-and-hole assembly process usually includes the following four steps: approach, hole location, one point contact and two point contact, which are categorized depending on the contact states. As shown in Figure 1.1, there are also two more contact states that can happen during the process: the other side one point contact and surface contact. There is also one additional possibility, that is when the peg is not touching the hole once already inside. But after it moves, it might jump to any other cases. In the following chapters, the different relationship between force and torque response and kinematics in each state would be derived in detail. Many assembly strategies utilize some technique by approaching from one side and maintaining contact with the edge of hole throughout the operation. Such a guided movement can reduce the possibility of losing track of contact states. So the forces and reactions can be easily analyzed within the same case.

2. BACKGROUND

This chapter will follow the analysis done by Simunovic [18] and Whitney [2] to provide some background knowledge about the peg-and-hole problem that is crucial to the problem this thesis is trying to solve, including the geometry and force analysis for each contact state, prediction of the position and rotation behavior during the peg-and-hole assembly, and why a passive compliance device like RCC would work. The major difference is that in this thesis an arbitrary compliance center position is used instead of a compliance center assumed to be on the center axis of the peg. Also similar to the work from Yamshita [6], how a simple active compliance approach can avoid jamming is discussed at the end.

2.1 Coordinates and Initial Error

To start the analysis, suppose a coordinate system C_P attached to the peg and another coordinate system C_H attached to the hole in Figure 2.1. The origin O_P is at the center of the end of the peg and the origin O_H is at the center of the top surface of the hole. Here, the $x-z$ plane of the C_P and the $x-z$ plane of C_H are co-aligned with the only rotational freedom allowed. Thus, in this case, the rotational error θ_y is defined as the angle from z_H to z_P. The radius of the peg is noted as r and the radius of the hole is noted as R.

When the peg is mounted on the robot arm, the force torque and position rotation relationship between these two can be represented by a compliance matrix. And such a matrix can be transformed to be a diagonal matrix or close to be a diagonal matrix, which is when the other terms are much smaller compared to diagonal terms, at a specific point, compliance center. In other words, force and torques passing through the compliance center will only result in translation or rotation movement in the

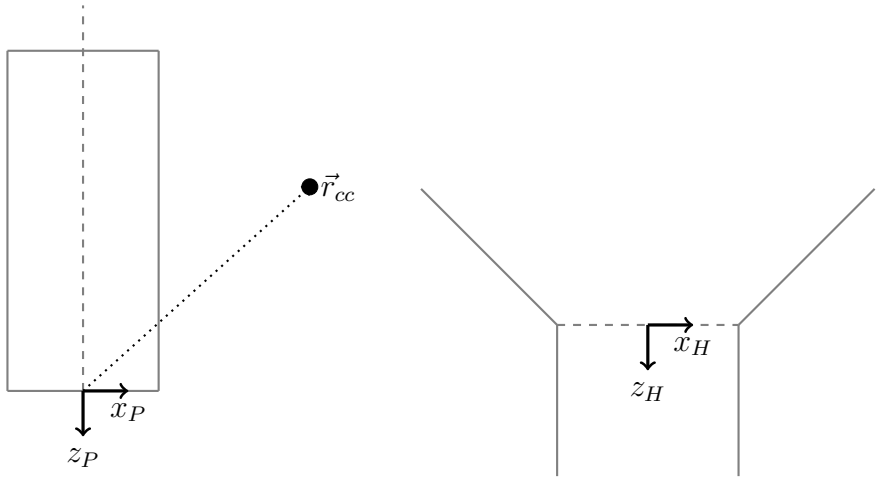

(a) Coordinate C_P (b) Coordinate C_H

Figure 2.1. : The Coordinate Systems for the Peg and the Hole

same direction. Here suppose the compliance center of the support on the peg is also in the $x - z$ plane for simplicity. This compliance center is noted as $\vec{r}_{cc}$ from O_P, corresponding to r_{ccx} along x_p and r_{ccz} along z_p. Here the r_{ccx} term is brought in to represent arbitrary compliance center location, while in most other compliance center analysis r_{ccx} is always assumed to be zero. The lateral stiffness along x_p is K_x and stiffness along z_p is K_z and the angular stiffness around y_p would be K_{R_y}. Therefore, the peg can be considered as connected to the end of the actuator by two springs and a torsion spring.

Figure 2.2 shows the initial condition for a general peg-and-hole problem. Due to hole location errors, for example from visions, and robot control accuracy limits, position and rotation error is unavoidable. Here the distance from the z_H axis to O_P along x_H direction is noted as ϵ_x, the distance from the z_H to the compliance center along x_H direction is noted as D_x and the distance from the x_H axis to the compliance center along z_H is noted as D_z. The initial values are noted as ϵ_{x0}, D_{x0} and D_{z0} accordingly. And the initial angle error θ_y is noted as θ_{y0}.

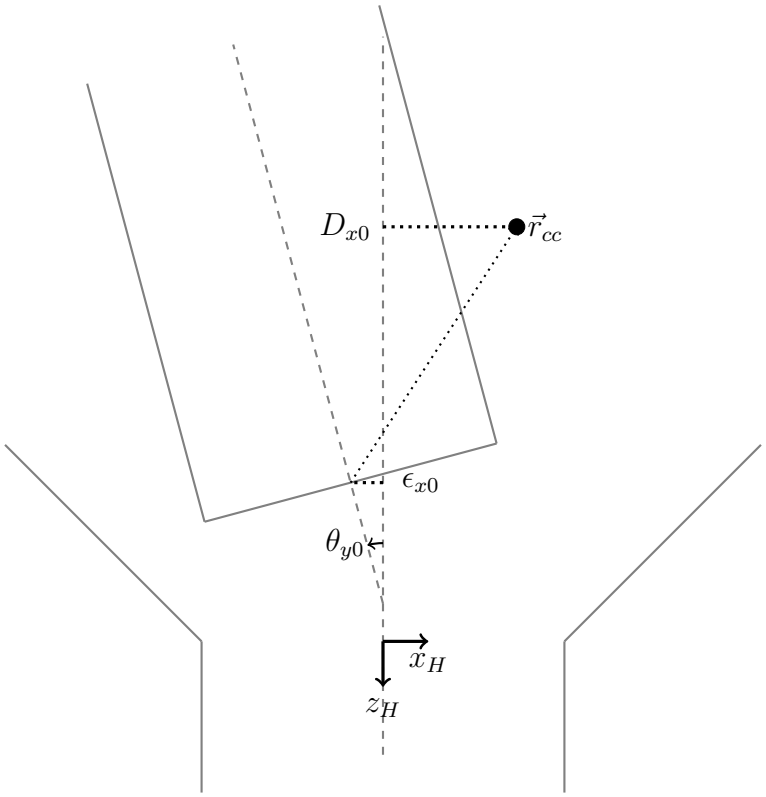

Figure 2.2. : Peg and Hole at Initial Position

So the relationship between D_x and ϵ_x is:

$$D_x = \epsilon_x + r_{ccx}\cos\theta_y + r_{ccz}\sin\theta_y \tag{2.1}$$

$$D_{x0} = \epsilon_{x0} + r_{ccx}\cos\theta_{y0} + r_{ccz}\sin\theta_{y0} \tag{2.2}$$

For a peg-and-hole problem, the error angle is usually small, so it is reasonable to use small angle approximation for θ_y. Therefore:

$$D_x = \epsilon_x + r_{ccx} + r_{ccz}\theta_y \tag{2.3}$$

$$D_{x0} = \epsilon_{x0} + r_{ccx} + r_{ccz}\theta_{y0} \tag{2.4}$$

Under quasi-static assumption,the force and torque the peg experienced can relate to the position and rotation changes as the following:

$$D_x = D_{x0} + T_x + \frac{F_x}{K_x}\cos\theta_y + \frac{F_z}{K_z}\sin\theta_y \tag{2.5}$$

$$D_z = D_{z0} + T_z + \frac{F_z}{K_z}\cos\theta_y - \frac{F_x}{K_x}\sin\theta_y \tag{2.6}$$

$$\theta_y = \theta_{y0} + R_y + \frac{M_y}{K_{R_y}} \tag{2.7}$$

T_x is the total displacement from the gripper relative to its initial position along x_H. T_z and R_y are the similar position and rotation caused by the robot end factor in C_H. In other words, T_x, T_z and R_y can be treated as position control reference inputs. Thus for a straight downwards movement using RCC, $T_x = R_y = 0$. And F_x, F_z and M_y are contact forces and corresponding torque about the compliance center caused by the hole under coordinates C_P in equilibrium state.

2.2 Chamfer Crossing

If the initial error for the peg isn't small enough for the peg to be inserted into the hole directly and isn't too large for the peg to completely miss the hole area, the peg would first make contact with the hole at the chamfer area. For the contact state of chamfer crossing, the tip of the peg would make contact with the chamfer surface and then be pushed towards the hole. There would be a normal reaction force f_1 from the chamfer and also a friction along the chamfer surface as shown in Figure 2.3. μ is the friction coefficient between the peg and the chamfer, α is the chamfer angle and s is the distance from the peg and chamfer contact point to the entrance of the hole. s_0 is used to denote s when the peg first touches the chamfer. So when there is no contact forces yet:

$$D_{x0} + T_x = (r + r_{ccx})\cos\theta_{y0} + r_{ccz}\sin\theta_{y0} - R - s_0\cos\alpha \tag{2.8}$$

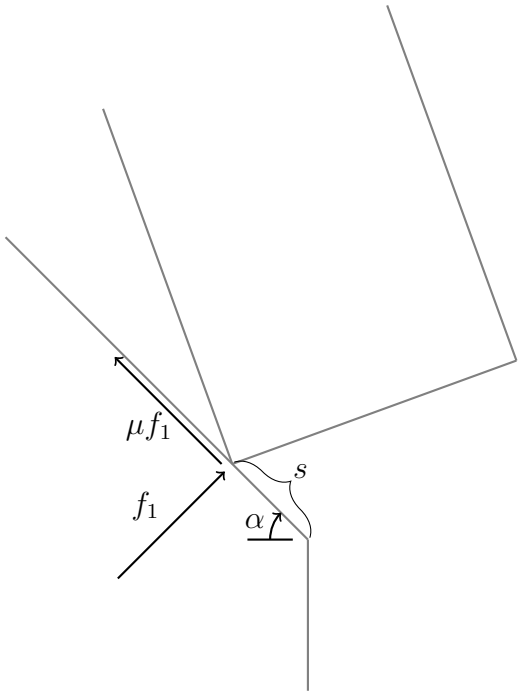

Figure 2.3. : Chamfer Crossing

During chamfer crossing, the resulted force and moment in coordinate C_P are:

$$F_x = f_1(\sin(\alpha + \theta_y) - \mu\cos(\alpha + \theta_y)) \tag{2.9}$$

$$F_z = -f_1(\cos(\alpha + \theta_y) + \mu\sin(\alpha + \theta_y)) \tag{2.10}$$

$$M_y\mathbf{j} = ((-r - r_{ccx})\mathbf{i} - r_{ccz}\mathbf{k}) \times (F_x\mathbf{i} + F_z\mathbf{k}) \tag{2.11}$$

With small angle approximation of θ_y:

$$F_x = f_1(\mathbf{B} + \mathbf{A}\theta_y) \tag{2.12}$$

$$F_z = -f_1(\mathbf{A} - \mathbf{B}\theta_y) \tag{2.13}$$

$$M_y = -(r_{ccz}(\mathbf{B} + \mathbf{A}\theta_y) + (r_{ccx} + r)(\mathbf{A} - \mathbf{B}\theta_y))f_1 \tag{2.14}$$

$$\mathbf{A} = \cos\alpha + \mu\sin\alpha \tag{2.15}$$

$$\mathbf{B} = \sin\alpha - \mu\cos\alpha \tag{2.16}$$

During chamfer crossing, the kinematics also give:

$$D_x = r + r_{ccx} + r_{ccz}\theta_y - R - s\cos\alpha \tag{2.17}$$

Plugging 2.12 & 2.13 into equation 2.5 and 2.14 into 2.7 would give:

$$D_x - D_{x0} - T_x = (\frac{\mathbf{B} + \mathbf{A}\theta_y}{K_x} - \frac{(\mathbf{A} - \mathbf{B}\theta_y)\theta_y}{K_z})f_1 \tag{2.18}$$

$$\theta_y - \theta_{y0} + R_y = -\frac{r_{ccz}(\mathbf{B} + \mathbf{A}\theta_y) + (r_{ccx} + r)(\mathbf{A} - \mathbf{B}\theta_y)}{K_{R_y}} f_1 \tag{2.19}$$

Combining them yields the relation between θ_y and s during chamfer crossing:

$$\frac{K_x K_z (D_x - D_{x0} - T_x)}{K_z(\mathbf{B} + \mathbf{A}\theta_y) - K_x(\mathbf{A} - \mathbf{B}\theta_y)\theta_y} = -\frac{K_{R_y}(\theta_y - \theta_{y0} - R_y)}{r_{ccz}(\mathbf{B} + \mathbf{A}\theta_y) + (r_{ccx} + r)(\mathbf{A} - \mathbf{B}\theta_y)} \tag{2.20}$$

It can be transformed into a cubic equation of θ_y about s, but the expression would make analysis too complicated for any good results. So this would only be used in numerically theoretical value prediction later on. For analysis, the small rotational difference between C_P and C_H would be neglected because θ_y is small. This is also the same assumption Whitney and Simunovic made in their papers. Later plots of the theoretical predictions would be presented to show how big a difference this assumption would cause.

Now if F_x and F_z are considered to be align with x_H and z_H, then:

$$F_x = f_1 \mathbf{B} \tag{2.21}$$

$$F_z = -f_1 \mathbf{A} \tag{2.22}$$

$$M_y \mathbf{j} = ((-r - r_{ccx})\mathbf{i} - r_{ccz}\mathbf{k}) \times (F_x \mathbf{i} + F_z \mathbf{k}) \tag{2.23}$$

Where $\mathbf{A}$ and $\mathbf{B}$ are the same as equations 2.15 and 2.16. Then M_y would be:

$$M_y = -(r_{ccz}\mathbf{B} + (r_{ccx} + r)\mathbf{A})f_1 \tag{2.24}$$

And since the rotational difference between C_P and C_H is ignored, the quasi-static equilibrium equations from 2.5 and 2.6 become:

$$D_x = D_{x0} + T_x + \frac{F_x}{K_x} \tag{2.25}$$

$$D_z = D_{z0} + T_z + \frac{F_z}{K_z} \tag{2.26}$$

Combination of equations 2.21, 2.17 and 2.25 gives:

$$f_1 = \frac{K_x}{\mathbf{B}}(r + r_{ccx} + r_{ccz}\theta_y - R - s\cos\alpha - D_{x0} - T_x) \tag{2.27}$$

Plug it and 2.7 into equation 2.24 and yield the relation between θ_y and s during chamfer crossing:

$$\theta_y = \frac{K_{R_y}(\theta_{y0} + R_y)\mathbf{B} - (r_{ccz}\mathbf{B} + (r_{ccx} + r)\mathbf{A})K_x(r - R + r_{ccx} - D_{x0} - T_x - s\cos\alpha)}{(r_{ccz}\mathbf{B} + (r_{ccx} + r)\mathbf{A})K_x r_{ccz} + K_{R_y}\mathbf{B}} \tag{2.28}$$

So θ_y is considered to be linear to s during chamfer crossing.

Now with equation 2.4, note $\epsilon'_x = \epsilon_x + R - r$:

$$r - R + r_{ccx} - D_{x0} - T_x = r - R + r_{ccx} - T_x - \epsilon_{x0} - r_{ccx}\cos\theta_{y0} - r_{ccz}\sin\theta_{y0} \tag{2.29}$$

$$= -\epsilon'_{x0} - T_x - r_{ccz}\theta_{y0} \tag{2.30}$$

So for the case of $s = 0$ in equation 2.28, θ_{yc}, the angle that chamfer crossing ends, would be:

$$\theta_{yc} = \theta_{y0} + \frac{K_{R_y}R_y\mathbf{B} + (r_{ccz}\mathbf{B} + (r_{ccx} + r)\mathbf{A})K_x(\epsilon'_{x0} + T_x)}{(r_{ccz}\mathbf{B} + (r_{ccx} + r)\mathbf{A})K_x r_{ccz} + K_{R_y}\mathbf{B}} \tag{2.31}$$

And the F_x, F_z and M_y force and torque sensor would detect if the peg maintains quasi-static movement in equilibrium state would be:

$$F_x = K_x(r_{ccz}\theta_y - r_{ccz}\theta_{y0} - s\cos\alpha - \epsilon'_{x0} - T_x) \tag{2.32}$$

$$F_z = -\frac{\cos\alpha + \mu\sin\alpha}{\sin\alpha - \mu\cos\alpha}F_x \tag{2.33}$$

$$M_y = -r_{ccz}F_x + (r_{ccx} + r)F_z \tag{2.34}$$

2.3 One Point Contact

After the peg slides across the chamfer and into the hole, the contact point would then shift to between the side of the peg and the edge of the hole at the entrance like in Figure 2.4. There would be a reaction force f_1 that is normal to the peg side and a friction force along the peg. μ here is the friction coefficient between the peg the hole. l is the length from the tip of the peg to the contact point along the peg. So l would indicate how deep the peg has already been inserted into the hole. Again, if

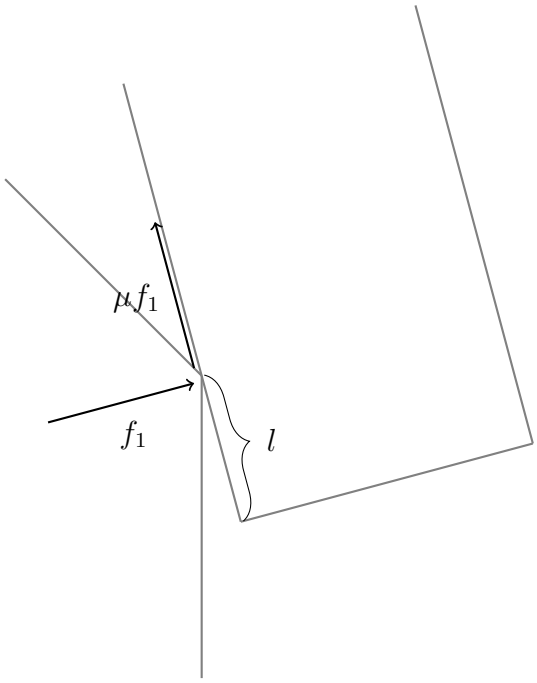

Figure 2.4. : One Point Contact

F_x and F_z can be considered as aligning with x_H and z_H, at one point contact, the resultant force and moment are:

$$F_x = f_1 \tag{2.35}$$

$$F_z = -\mu f_1 \tag{2.36}$$

$$M_y\mathbf{j} = ((-r - r_{ccx})\mathbf{i} + (-l - r_{ccz})\mathbf{k}) \times (F_x\mathbf{i} + F_z\mathbf{k}) \tag{2.37}$$

So M_y would be:

$$M_y = -(\mu r + \mu r_{ccx} + l + r_{ccz})f_1 \tag{2.38}$$

At one point contact, the kinematics also indicates:

$$D_x = l\theta_y + r - R + r_{ccx} + r_{ccz}\theta_y \tag{2.39}$$

$$D_z = l - r\theta_y - r_{ccx}\theta_y + r_{ccz} \tag{2.40}$$

Combination of equations 2.35, 2.39 and 2.25 gives:

$$f_1 = K_x(l\theta_y + r - R + r_{ccx} + r_{ccz}\theta_y - D_{x0} - T_x) \tag{2.41}$$

Plug it and equation 2.38 into 2.7 and yield the relation between θ_y and l during one point contact:

$$\theta_y = \frac{K_{R_y}(\theta_{y0} + R_y) - (\mu r + \mu r_{ccx} + l + r_{ccz})K_x(r - R + r_{ccx} - D_{x0} - T_x)}{(\mu r + \mu r_{ccx} + l + r_{ccz})K_x(l + r_{ccz}) + K_{R_y}} \tag{2.42}$$

So for the case of $l = 0$ in equation 2.42, combining with 2.30, θ_{y1}, the angle that one point contact begins, would be:

$$\theta_{y1} = \theta_{y0} + \frac{K_{R_y}R_y + (\mu r + \mu r_{ccx} + r_{ccz})K_x(\epsilon'_{x0} + T_x)}{(\mu r + \mu r_{ccx} + r_{ccz})K_x r_{ccz} + K_{R_y}} \tag{2.43}$$

And the F_x, F_z and M_y force and torque sensor would detect if the peg maintains quasi-static movement in equilibrium state would be:

$$F_x = K_x(l\theta_y + r_{ccz}\theta_y - r_{ccz}\theta_{y0} - \epsilon'_{x0} - T_x) \tag{2.44}$$

$$F_z = -\mu F_x \tag{2.45}$$

$$M_y = -(l + r_{ccz})F_x + (r + r_{ccx})F_z \tag{2.46}$$

2.4 Two Point Contact

As the peg slides inwards while maintaining one point contact with the left edge of the hole, the peg might keep rotating due to initial position and angle error to a point that the peg will touch the other side of the hole, like in Figure 2.5. In such a case, there are two normal reaction forces f_1 and f_2 as well as corresponding friction forces. l and μ are the same definition as one point contact. The geometry constraints of two point contact gives:

$$l \sin\theta_y + 2r\cos\theta_y = 2R \tag{2.47}$$

With small angle approximation, the relationship between θ_y and l during two point contact should hold as:

$$l\theta_y = 2R - 2r \tag{2.48}$$

At the time that two point contact initially occurs or is just about to end, as the other side of the peg is barely touching the hole, it is safe to assume there is no

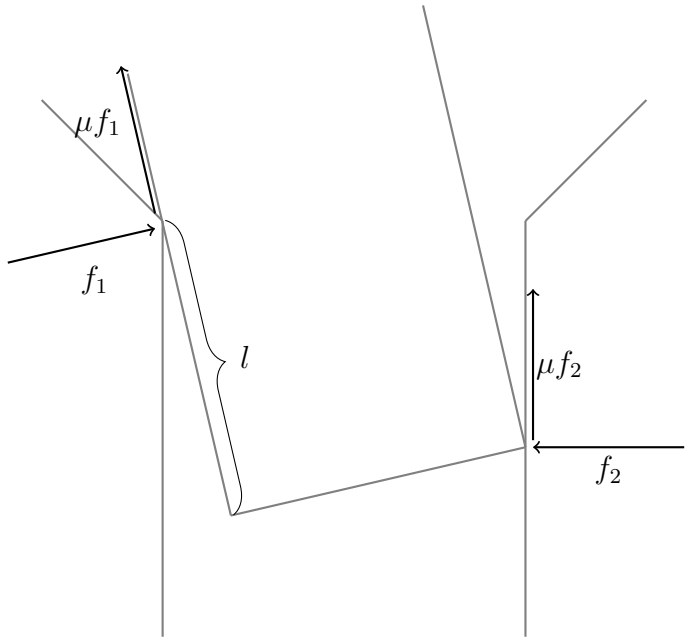

Figure 2.5. : Two Point Contact

contact force on the other side, that is $f_2 = 0$. So the conclusion for θ_y and l from one point contact is also valid at that time. Thus after combining equations 2.48 and 2.42, the solution to the following equation indicates l for the start and the end of two point contact:

$$\alpha l^2 + \beta l + \gamma = 0 \tag{2.49}$$

Here:

$$\alpha = K_x(r - R + D_{x0} + T_x - r_{ccx}) \tag{2.50}$$

$$\beta = K_{R_y}(\theta_{y0} + R_y) + \alpha(r_{ccz} + \mu r + \mu r_{ccx}) + (2r - 2R)K_x r_{ccz} \tag{2.51}$$

$$\gamma = (2r - 2R)(K_{R_y} + K_x r_{ccz}(r_{ccz} + \mu r + \mu r_{ccx})) \tag{2.52}$$

When $\Delta = \beta^2 - 4\alpha\gamma > 0$, there are two different solutions to equation 2.49. The smaller one will be noted as l_2, the start of two point contact. And the bigger one will be noted as l_2', the end of two point contact and back to continue as one point contact. Or in some cases, the θ_y with respect to the l_2' is very to zero, then with some compliance center locations and F_x the peg will snap from two point contact to surface

contact. When $\Delta = 0$, two point contact barely takes place and the whole process may be studied as one point contact. Basically, the clearance is just as large as how far the other side of the tip can reach during one point contact. And when $\Delta < 0$, two point contact may not happen. In section 2.5, it will be shown that jamming and wedging, two major causes of peg-and-hole assembly failure, occur mostly during two point contact. Here it will be explained how RCC would be able to help avoid two point contact phase and thus make peg-and-hole assembly trivial.

With equation 2.4, note $\epsilon''_x = \epsilon_x + r - R$:

$$r - R + D_{x0} + T_x - r_{ccx} = r - R + \epsilon_{x0} + r_{ccx} + r_{ccz}\sin\theta_{y0} + T_x - r_{ccx} \tag{2.53}$$

$$= \epsilon''_{x0} + T_x + r_{ccz}\theta_{y0} \tag{2.54}$$

Suppose a passive compliance device, Remote Compliance Center, can have the compliance center to be roughly at the same point of O_P. That is ideally $r_{ccx} = r_{ccz} = 0$. And then α would be:

$$\alpha = K_x(\epsilon''_{x0} + T_x) \tag{2.55}$$

And let $T_x = R_y = 0$, then the discriminant would be:

$$\Delta = \beta^2 - 4\alpha\gamma \tag{2.56}$$

$$= (K_{R_y}\theta_{y0} + K_x\epsilon''_{x0}\mu r)^2 - 4K_x\epsilon''_{x0}(2r - 2R)K_{R_y} \tag{2.57}$$

Now if $K_{R_y}\theta_{y0} >> \mu K_x\epsilon''_{x0}r$ is assumed just like Whitney did in his paper, which is easily met in common real world RCC devices with small initial errors, then:

$$\Delta \cong K_{R_y}(K_{R_y}\theta^2_{y0} + 8(R - r)K_x\epsilon''_{x0}) \tag{2.58}$$

The hole radius R would need to be bigger than peg radius r for the assembly to be possible. K_{R_y} and K_x are stiffness that would be of a positive value. And $\epsilon''_{x0} = \epsilon_{x0} + r - R$ would be negative if $\epsilon_{x0} < 0$. In this case, the initial position of the center of the peg's end is to the left of the hole. Therefore, Δ would be negative when θ_{y0} is small. In other words, two point contact cannot happen with such a RCC

device when the initial errors are small even without additional control input other than move downwards along z_P.

When $\Delta \geq 0$, the starting and ending insert depth l_2 and l_2' under a RCC passive device can be estimated as the following.

At l_2 and its corresponding angle θ_{y2}, the right side of the peg is barely touching, so the analysis for f_1 under one point contact phase is still valid. And with equation 2.48, equation 2.41 becomes:

$$f_1 = K_x(R - r + r_{ccx} + r_{ccz}\theta_y - D_{x0} - T_x) \tag{2.59}$$

$$= K_x(-\epsilon''_{x0} - r_{ccz}\theta_{y0} + r_{ccz}\theta_y - T_x) \tag{2.60}$$

Similar to the process leading to equation 2.42, equations 2.38, 2.7 and 2.60 yield θ_{y2}:

$$\theta_{y2} = \frac{K_{R_y}(\theta_{y0} + R_y) + (\mu r + \mu r_{ccx} + l_2 + r_{ccz})K_x(\epsilon''_{x0} + r_{ccz}\theta_{y0} + T_x)}{(\mu r + \mu r_{ccx} + l_2 + r_{ccz})K_x r_{ccz} + K_{R_y}} \tag{2.61}$$

And for ideal RCC device with control input $T_x = R_y = 0$:

$$\frac{2R - 2r}{l_2} = \frac{K_{R_y}\theta_{y0} + (\mu r + l_2)K_x\epsilon''_{x0}}{K_{R_y}} \tag{2.62}$$

From previous assumption $K_{R_y}\theta_{y0} >> \mu K_x\epsilon''_{x0} r$ and the common case that l_2 should have roughly same or even smaller magnitude of μr, the starting insert depth of two point contact phase would be:

$$l_2 \cong \frac{2R - 2r}{\theta_{y0}} \tag{2.63}$$

And:

$$l_2 + l_2' = -\frac{\beta}{\alpha} = \frac{K_{R_y}(\theta_{y0} + R_y) + \alpha(r_{ccz} + \mu r + \mu r_{ccx}) + (2r - 2R)K_x r_{ccz}}{K_x(r - R + \epsilon_{x0} + r_{ccz}\theta_{y0} + T_x)} \tag{2.64}$$

$$= \frac{K_{R_y}\theta_{y0} + K_x\epsilon''_{x0}\mu r}{K_x\epsilon''_{x0}} \tag{2.65}$$

$$\cong \frac{K_{R_y}\theta_{y0}}{K_x\epsilon''_{x0}} \tag{2.66}$$

So the ending insert depth of two point contact phase would be:

$$l_2' \cong \frac{K_{R_y}\theta_{y0}}{K_x\epsilon''_{x0}} - \frac{2R - 2r}{\theta_{y0}} \tag{2.67}$$

2.5 Jamming and Wedging

Jamming is the term used to describe the case that peg is not moving because of the applied force and torque having the wrong magnitude. In such a scenario, much bigger force or torque would be required to keep the peg moving, or the proportion and orientation of the applied force would need to changed due to the previously applied is causing the peg to jam into the side to the hole, or rotate more inside the hole instead of move inwards.

A plot of $\frac{M_y}{F_z}$ versus $\frac{F_x}{F_z}$ will be made to show how the combination of the forces and moments applied to the peg would affect the states of the peg and the hole. The angle difference of contact forces along the peg and along the hole will be ignored in all jamming analysis here for a simpler and clearer result. First, the force and moment the peg would experience during two point contact equilibrium state as in Figure 2.5 is considered:

$$F_x = f_1 - f_2 \tag{2.68}$$

$$F_z = -\mu f_1 - \mu f_2 \tag{2.69}$$

$$\begin{aligned} M_y\mathbf{j} =& (-(r + r_{ccx})\mathbf{i} - (l + r_{ccz})\mathbf{k})) \times (f_1\mathbf{i} - \mu f_1\mathbf{k}) \\ &+ ((r - r_{ccx})\mathbf{i} - r_{ccz}\mathbf{k})) \times (-f_2\mathbf{i} - \mu f_1\mathbf{k}) \end{aligned} \tag{2.70}$$

So M_y is:

$$M_y = -(\mu r + \mu r_{ccx} + l + r_{ccz})f_1 - (\mu r_{ccx} - r_{ccz} - \mu r)f_2 \tag{2.71}$$

Combining equations 2.68, 2.69 and 2.71 would yield the relationship between $\frac{M_y}{F_z}$ and $\frac{F_x}{F_z}$ during two point contact equilibrium state:

$$\frac{M_y}{F_z} = (-\mu r - r_{ccz} - \frac{l}{2})\frac{F_x}{F_z} + (r_{ccx} + \frac{l}{2\mu}) \tag{2.72}$$

And when the peg and the hole is at one point contact on the left side as in Figure 2.4, the combination of F_x, F_z and M_y can be deducted from equations 2.45 and 2.46:

$$\frac{F_x}{F_z} = -\frac{1}{\mu} \tag{2.73}$$

$$\frac{M_y}{F_z} = \frac{\mu r + \mu r_{ccx} + l + r_{ccz}}{\mu} \tag{2.74}$$

And when the peg and the hole is at the other side one point contact as shown in Figure 1.1e, $\theta_y > 0$ and the force and torque may be considered the same as in Figure 2.5 except $f_1 = 0$:

$$F_x = -f_2 \tag{2.75}$$

$$F_z = -\mu f_2 \tag{2.76}$$

$$M_y\mathbf{j} = ((r - r_{ccx})\mathbf{i} - r_{ccz}\mathbf{k})) \times (-f_2\mathbf{i} - \mu f_1\mathbf{k}) \tag{2.77}$$

So M_y is:

$$M_y = -(\mu r_{ccx} - r_{ccz} - \mu r) f_2 \tag{2.78}$$

Thus the combination of F_x, F_z and M_y at this state would be:

$$\frac{F_x}{F_z} = \frac{1}{\mu} \tag{2.79}$$

$$\frac{M_y}{F_z} = \frac{\mu r_{ccx} - r_{ccz} - \mu r}{\mu} \tag{2.80}$$

However, for the two point contact while $\theta_y < 0$, which is the mirror case of two point contact in Figure 2.5, the force and moment the peg would experience during two point contact equilibrium state would then be:

$$F_x = f_1 - f_2 \tag{2.81}$$

$$F_z = -\mu f_1 - \mu f_2 \tag{2.82}$$

$$\begin{aligned} M_y\mathbf{j} =& (-(r + r_{ccx})\mathbf{i} - r_{ccz}\mathbf{k})) \times (f_1\mathbf{i} - \mu f_1\mathbf{k}) \\ &+ ((r - r_{ccx})\mathbf{i} - (l + r_{ccz})\mathbf{k})) \times (-f_2\mathbf{i} - \mu f_2\mathbf{k}) \end{aligned} \tag{2.83}$$

So M_y is:

$$M_y = -(\mu r + \mu r_{ccx} + r_{ccz})f_1 - (\mu r_{ccx} - l - r_{ccz} - \mu r)f_2 \tag{2.84}$$

Combining the above equations yields the relationship during opposite two point contact equilibrium state:

$$\frac{M_y}{F_z} = (-\mu r - r_{ccz} - \frac{l}{2})\frac{F_x}{F_z} + (r_{ccx} - \frac{l}{2\mu}) \tag{2.85}$$

Similar to how equations 2.79 and 2.80 are generated from the two point contact state, by setting $f_1 = 0$ and $f_2 = 0$ separately in the opposite two point contact equations, the following combinations of F_x, F_z and M_y are achieved for the rest two one point contact state while $\theta_y < 0$:

$$\frac{F_x}{F_z} = \frac{1}{\mu} \tag{2.86}$$

$$\frac{M_y}{F_z} = \frac{-\mu r + \mu r_{ccx} - l - r_{ccz}}{\mu} \tag{2.87}$$

And:

$$\frac{F_x}{F_z} = -\frac{1}{\mu} \tag{2.88}$$

$$\frac{M_y}{F_z} = \frac{\mu r_{ccx} + r_{ccz} + \mu r}{\mu} \tag{2.89}$$

Putting all of the above $\frac{M_y}{F_z}$ and $\frac{F_x}{F_z}$ together generates the jamming diagram shown in Figure 2.6. The top line indicates the relationship between forces for the peg to slide in maintaining two point contact when θ_y is positive. The leftmost circle is when only the peg body is touching the left edge of the hole and the rightmost circle is when only the peg tip is touching the right side of the hole. And the bottom line is the symmetrical which is when θ_y is negative. The left and right dashed line indicates when the peg side is having surface contact with the hole side. When the force and moment applied falls inside this parallelogram, the peg will accelerate and fall into the hole. However, the force and moment applied outside would result in a jamming. Which means that the additional applied force or moment is causing the

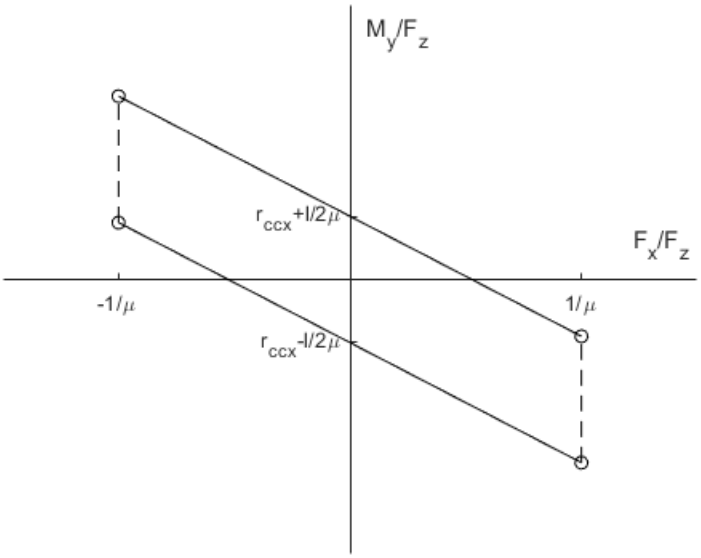

Figure 2.6. : Jamming Diagram

peg to hit the wall inside the hole instead of move inwards. This diagram shows that, as the peg moves in, l gets bigger, the parallelogram will expand vertically and the allowed region for force and moment without causing a jamming would be bigger. It also indicates that increasing F_z would help the assembly process. But this is not always true because M_y could be also increasing. The diagram is plotted assuming $r_{ccx} = 0$ and $R_{ccz} = 0$. The actual slope of the two point contact equilibrium is $-\mu r - r_{ccz} - \frac{l}{2}$, while the axis intercept is $r_{ccx} \pm \frac{l}{2\mu}$. Thus, changing r_{ccx} will move the diagram upwards or downwards and changing r_{ccz} will cause the top and bottom line to rotate about their $\frac{M_y}{F_z}$ axis intercept.

Wedging is the case that the peg would stop moving inside the hole while building up internal forces. It is caused by geometry and in some cases cannot be broken out by applying any proportion of forces and torques without damaging or deforming the parts. It happens when the insertion depth is small and the friction core $\tan \phi' = \mu$ is large enough to allow two reaction forces to be aligned in the exact opposite direction.

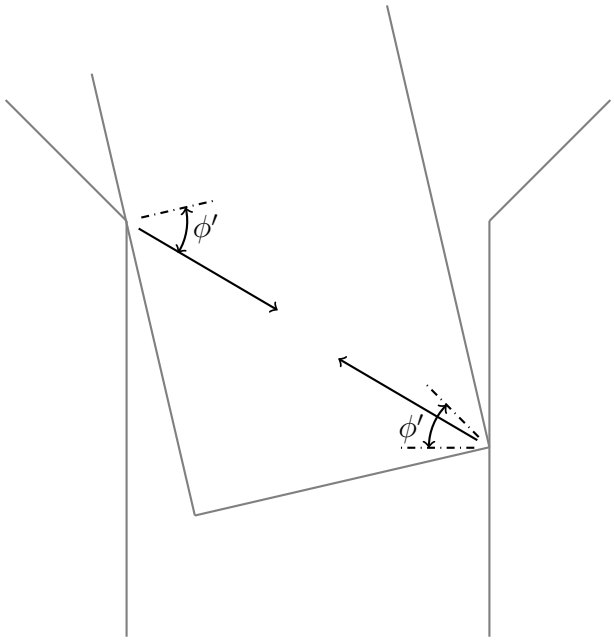

Figure 2.7. : Wedging

At such time, if the peg was pushed counterclockwise and would like to be released from this pose, the forces from the hole would not be able to help achieve that. And to form this state, the insert depth will need to be:

$$\frac{l}{2r} \leq \mu \tag{2.90}$$

And since wedging also requires two point contact, it would mean that wedging can occur only if:

$$l_2 \leq 2\mu r \tag{2.91}$$

With equation 2.48, the above is equivalent to wedging would not happen if:

$$|\theta_{y2}| < \frac{R-r}{\mu r} \tag{2.92}$$

And from equation 2.61, assume l, μr and μr_{ccx} are small:

$$\theta_{y2} = \frac{K_{R_y}(\theta_{y0} + R_y) + r_{ccz}K_x(\epsilon''_{x0} + r_{ccz}\theta_{y0} + T_x)}{K_x r_{ccz}^2 + K_{R_y}} \tag{2.93}$$

So for $T_x = R_y = 0$, the initial condition to avoid wedging is:

$$-\frac{R-r}{\mu r} < \theta_{y0} + \frac{r_{ccz}K_x}{K_x r_{ccz}^2 + K_{R_y}}\epsilon''_{x0} < \frac{R-r}{\mu r} \tag{2.94}$$

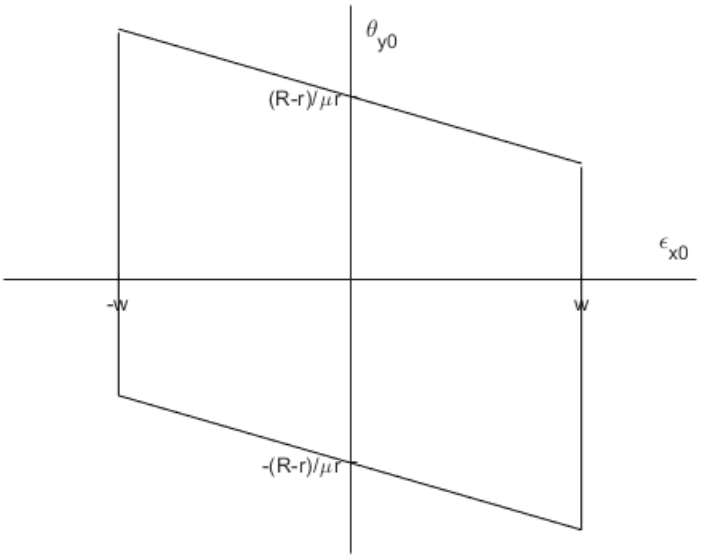

Figure 2.8. : Geometry Contraints for Initial Error

Also, in order to let the peg cross chamfer area, ϵ_{x0} needs to be bounded:

$$-w < \epsilon_{x0} < w \tag{2.95}$$

Here w is the horizontal width of the chamfer area. And assuming the difference between ϵ''_{x0} and ϵ_{x0} is small, the initial error for the peg to be safely inserted can be plotted as within the parallelogram in Figure 2.8.

2.6 l-θ Plot

Equation 2.42 provides the relationship between θ_y and l during one point contact, which shall be valid from $l = 0$ to $\theta_y = 0$. Equation 2.48 indicates the relationship between θ_y and l during two point contact, which, if the discriminant is positive, shall be valid from l_2 to l'_2. And if, during the chamfer crossing phase, the l is defined as $-s\tan\alpha$, the relationship θ_y and l can be shown with equation 2.28. Here, Figure

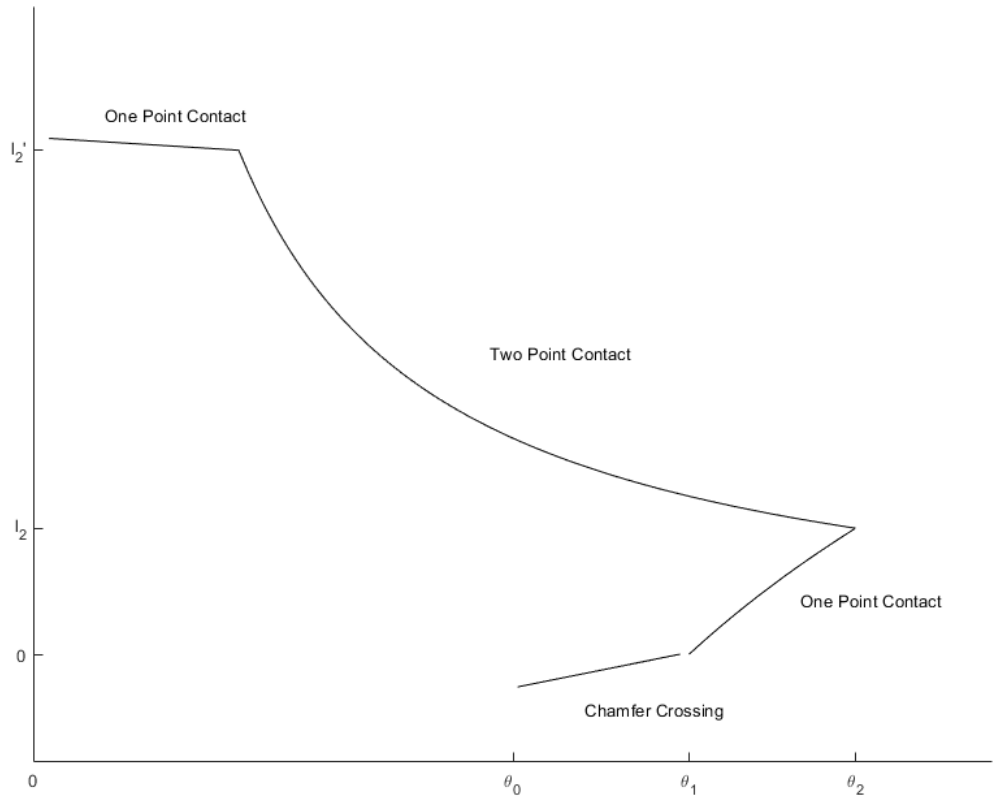

Figure 2.9. : l-θ Plot for Peg-and-hole assembly

2.9 shows the typical l versus θ during the whole assembly process for some initial setups.

In the above plot there is also a theta value jump for $l = 0$ between one point contact and chamfer crossing. This is due to the solution of θ_y when assuming $s = 0$ in the chamfer crossing phase differs from when assuming $l = 0$ in one point contact phase. The first one, θ_{yc} shown in equation 2.31, is set under assuming the contact force to be normal to the chamfer, while the second one, θ_{y1} shown in equation 2.43, is set under assuming the contact force to be normal to the side of the peg.

2.7 Passive Compliance

Apart from how RCC devices can avoid two point contact discussed earlier, the jamming diagram and l-θ plot also help show that the maximum F_z required to insert the peg would be bounded with the help of RCC. The force and moments that caused by control input while $T_x = 0$ and $R_y = 0$ and assuming F_x and F_z align with x_H and z_H would be:

$$F_x = K_x(D_{x0} - D_x) \tag{2.96}$$

$$F_z = K_z(D_{z0} + T_z - D_z) \tag{2.97}$$

$$M_y = K_{R_y}(\theta_{y0} - \theta_y) \tag{2.98}$$

As equations 2.48 and 2.39 indicate, F_x is limited and mostly determined by initial error D_{x0}. And as shown in the l-θ plot, the value of θ_y is pretty limited throughout the assembly process. At the meantime, increasing T_z can increase F_z, easily leading to $\frac{M_y}{F_z}$ and $\frac{F_x}{F_z}$ within the jamming parallelogram in the case of $r_{ccx} = r_{ccz} = 0$.

2.8 Active Compliance

Apart from algorithms that utilizes the geometry and force information discussed above to figure out the current contact state of the peg and provide the necessary force and moment for the peg to slide in, there are also simple force control strategies by setting a virtual compliance reference point. In Yamashita's paper, a jamming condition during two point contact while maintaining constant force pushing down-

wards is discussed. First, the total force and moment on the peg in C_P during two point contact would be:

$$F_x = f_1 - f_2 \cos\theta_y + \mu f_2 \sin\theta_y \tag{2.99}$$

$$F_z = -\mu f_1 - f_2 \sin\theta_y - \mu f_2 \cos\theta_y \tag{2.100}$$

$$\begin{aligned} M_y\mathbf{j} =& (-(r + r_{ccx}\mathbf{i} - (l + r_{ccz})\mathbf{k})) \times (f_1\mathbf{i} - \mu f_1\mathbf{k}) \\ &+ ((r - r_{ccx})\mathbf{i} - r_{ccz}\mathbf{k}) \times ((-f_2 \cos\theta_y + \mu f_2 \sin\theta_y)\mathbf{i} - (f_2 \sin\theta_y + \mu f_2 \cos\theta_y)\mathbf{k}) \end{aligned} \tag{2.101}$$

And if the reference force direction is set in the hole coordinates frame as in Yamshita's work, then:

$$F_{x_{\text{REF}}} = -F_{z_{\text{constant}}} \sin\theta_y \tag{2.102}$$

$$F_{z_{\text{REF}}} = F_{z_{\text{constant}}} \cos\theta_y \tag{2.103}$$

$$M_{y_{\text{REF}}} = 0 \tag{2.104}$$

If the above force and moment reference are met when $\theta_y > 0$, the force control will reach an equilibrium state and stop moving the peg, resulting in a jam. In such case, the forces are:

$$F_x = -F_{z_{\text{constant}}} \sin\theta_y \tag{2.105}$$

$$F_z = F_{z_{\text{constant}}} \cos\theta_y \tag{2.106}$$

And combine with equations 3.17 and 3.18 and rearrange:

$$f_2 = (\cos\theta_y - \mu \sin\theta_y) f_1 \tag{2.107}$$

From geometry constraint during two point contact(rearranged from equation 2.47):

$$l = (2R - 2r\cos\theta_y)/\sin\theta_y \tag{2.108}$$

Plug 3.29 and 3.30 into 3.20:

$$\begin{aligned} &(-\mu r - \mu r_{ccx} - \frac{2R - 2r\cos\theta_y}{\sin\theta_y} - r_{ccz}) \\ &\quad + ((r - r_{ccx})(\sin\theta_y + \mu\cos\theta_y) + r_{ccz}\cos\theta_y - \mu r_{ccz}\sin\theta_y)(\cos\theta_y - \mu\sin\theta_y) = 0 \end{aligned} \tag{2.109}$$

Which can be rearrange as:

$$\begin{aligned}\frac{R}{r} =&\alpha\frac{\sin\theta_y(-2\mu\sin\theta_y\cos\theta_y+(\mu^2-1)\sin^2\theta_y)}{2}\\ &+\beta\frac{-\mu\sin\theta_y-\sin\theta_y(\cos\theta_y-\mu\sin\theta_y)(\sin\theta_y+\mu\cos\theta_y)}{2}\\ &+\frac{\sin\theta_y(\cos\theta_y-\mu\sin\theta_y)(\sin\theta_y+\mu\cos\theta_y)-\mu\sin\theta_y+2\cos\theta_y}{2}\end{aligned} \tag{2.110}$$

Where:

$$\alpha = \frac{r_{ccz}}{r} \tag{2.111}$$

$$\beta = \frac{r_{ccx}}{r} \tag{2.112}$$

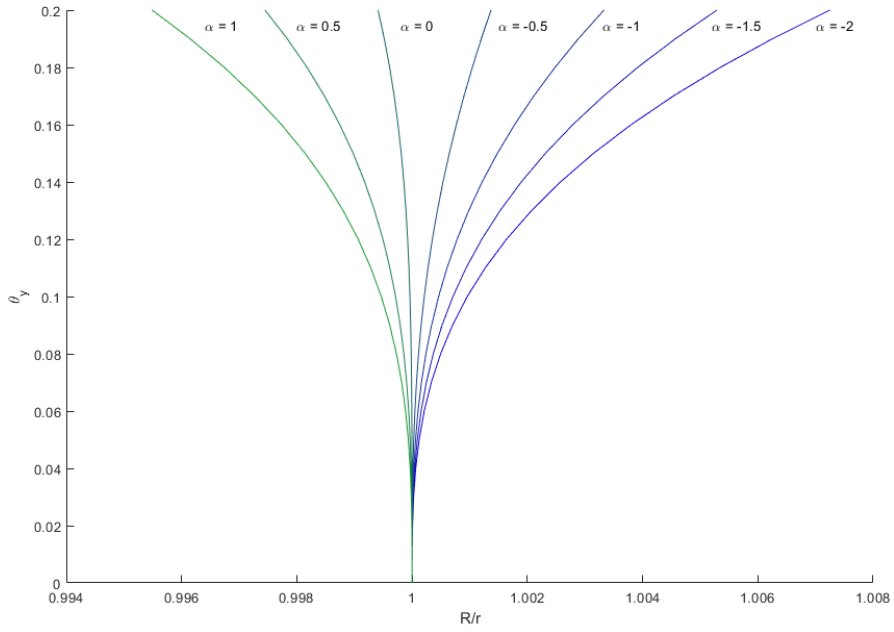

Figure 2.10. : Jamming Angle versus Radius Ratio when $\mu = 0$ for Various α

If $r_{ccx} = 0$, Figure 2.10 shows the jamming angles for different r_{ccz} values when $\mu = 0$. It can be seen that for $\alpha \geq 0$, no jamming solution exists for $R > r$. Also partial derivative assuming $r_{ccx} = 0$ gives:

$$\frac{\partial(\frac{R}{r})}{\partial\mu} = \sin\theta_y(\alpha(-\sin\theta_y\cos\theta_y+\mu\sin^2\theta_y)-(\sin^2\theta_y-\mu\sin\theta_y\cos\theta_y)) \tag{2.113}$$

For $\alpha \geq 0$, $\mu \geq 0$ and $\theta_y > 0$, the above partial derivative is always negative if $\mu < \cot \theta_y$. This condition would be easily met for reasonable friction coefficient μ and small initial angle error θ_y. So when μ gets bigger, the $\alpha \geq 0$ lines in the plot will lean more to the left and thus still no jamming solution exists for $R > r$.

So the previous conclusion is valid for all $\mu \geq 0$. In other words, when $r_{ccz} \geq 0$, which means the compliance center is below and outside the peg, such force control to push peg downwards will not result in a jamming equilibrium. This proves that placing the compliance center at the tip of the peg for force control active compliance is a good idea.

3. PROBLEM

This part would discuss the cases of $r_{ccx} \neq 0$ and show its effect on previous analysis. An active control strategy to cancel out its effect and to help passive compliance device insertion with an arbitrary compliance center is discussed. A specific case of peg being gripped at an error angle would be studied. And a r_{ccx} estimation strategy for this case is provided at the end.

3.1 Peg Gripped at an Error Angle

Here a specific off compliance center case with large r_{ccx} would be discussed. Such compliance center location can happen in the real life, can cause failure of the peg-and-hole assembly and can be estimated fairly easily. Suppose a scenario that requires a robot to pick up a peg and then insert it into a hole. Vision is used to locate the peg and the hole. In the real world, uncertainties are unavoidable during the process. In the previous chapter, ϵ_{x0} and θ_{y0} represent the error before inserting starts between the peg and the hole. And if the peg is not mounted firmly on the robot arm, error between the peg and the gripper would exist as well. And for a passive compliance device that is calibrated for the peg being ideally gripped, the error would then lead to the compliance center not at where the peg actually is. And in such case, the off compliance center and the compliance matrix would still be fixed relative to the peg during the assembly, so the arbitrary compliance center analysis from the previous chapter would still apply.

Now consider the case that the uncertainties from vision is much larger than the ones from robot arm sensors and actuators, which can be caused by using a single 2-D camera. Lighting limitations, object features and pixel resolutions can all result in errors of position and orientation estimation. For this thesis, a peg gripped at an

error angle case will be focused. Suppose that a gripper that is configured to have a Remote Compliance Center set up ideally at the end of the peg grabbed a peg with some error angle, like in Figure 3.1. The vision was able to ensure the uncertainties of θ_{y0} and ϵ_{x0} to be inside the parallelogram in Figure 2.8 to avoid wedging and cross chamfer. Due to additional uncertainties from the peg being picked up, visual servo strategy would be used to make sure the errors would not accumulate to have the peg completely miss the hole area. Basically, visual servo uses the pixel difference feedback to control so the error from peg being imperfectly gripped would be vastly canceled when peg is being aligned to the hole [19]. For this reason, without additional control input, the move downwards can be regarded as the same before.

Also, since large uncertainty from vision is assumed and the orientation of the hole, which would be used to determine the direction to move downwards, is also estimated by vision, control input T_x that was zero would probably be a small nonzero value in the new case. But the difference it might cause would highly depend on the location where vision put the peg at and the ratio between K_x and K_z. If the peg is ended up distant to the hole and the vision estimated orientation error is huge, the peg can completely miss the chamfer area while the robot moves it closer and sideways at the same time, which means a whole different problem to be solved. On the other hand, if K_z is large, the additional motion along x_H will be hardly noticeable until the insert depth gets bigger. And as discussed in the jamming diagram part, jamming is less likely to happen when the insert depth is large. So in this thesis, the additional T_x that will be caused by the hole orientation estimation error will be ignored.

The mass of the peg is also assumed to be relatively small compared to the gripper device mounted on the passive compliance device. That is the change of gravity center from such a small angle error of the peg could be ignored and would not cause additional reaction torques or angle errors.

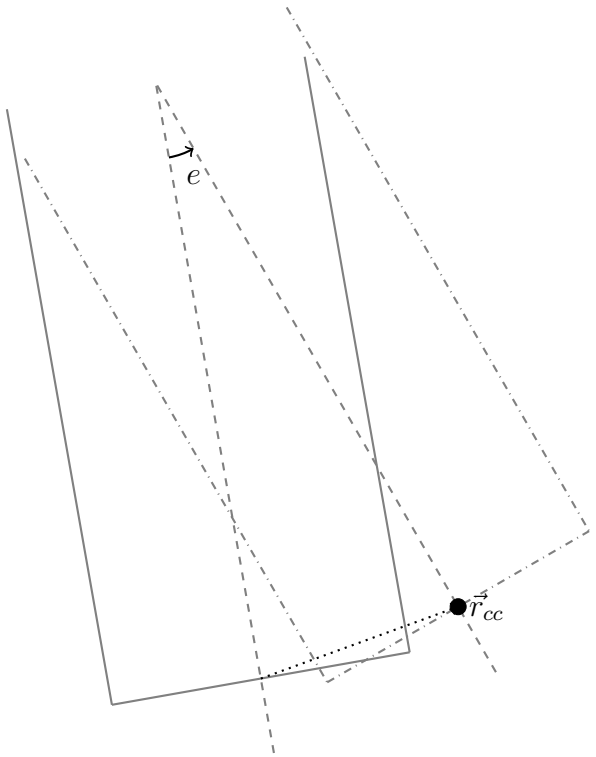

Figure 3.1. : Peg Gripped at an Error Angle

Starting with the peg gripped at an error angle, the new compliance center relative to the current peg tip center would be:

$$r'_{ccx} = (L_g + r_{ccz}) \sin e + r_{ccx} \cos e \tag{3.1}$$

$$r'_{ccz} = (L_g + r_{ccz}) \cos e - L_g - r_{ccx} \sin e \tag{3.2}$$

Here e is the error angle from current peg to ideal peg orientation and L_g is the length from where the gripper connects the peg to the end of the peg. It can be inferred that with originally an ideal or close to ideal compliance center, the r'_{ccz} would still be small but r'_{ccx} could be somewhat large. Later it will be shown that, even with a relatively small angle error, but with a long peg, the compliance center relative to the current peg center could be distant enough to cause issues during the assembly even if the same control strategies are used. In conclusion, the peg grabbed

at an error angle case, with the previous assumptions, would behave like a peg being inserted with normal control input except that r_{ccx} is large.

3.2 Off Compliance Center

The analysis in two point contact and jamming diagram in previous chapter has shown that a RCC device that places compliance center at the tip of the peg, which means letting $r_{ccz} = r_{ccx} = 0$, can avoid two point contact phase and get out jamming by increasing the force pushing downwards without any additional control input. It is also shown in the previous chapter that placing the virtual compliance center to be outside the peg, which means letting $r_{ccz} \geq 0$ and $r_{ccx} = 0$, can avoid jamming during two point contact phase for a force control active compliance strategy. However, even with keeping $r_{ccz} = 0$, just changing r_{ccx} values will lead to the previous conclusions invalid for some setups.

3.2.1 Two Point Contact

The discriminant for equation 2.49, two point contact starting and ending insert depth, when $r_{ccx} \neq 0$ but still assuming $r_{ccz} = 0$ and $T_x = R_y = 0$, would be:

$$\begin{aligned}\Delta =& \beta^2 - 4\alpha\gamma && (3.3)\\ =& (K_{R_y}\theta_{y0} + K_x(r - R + D_{x0} - r_{ccx})(\mu r + \mu r_{ccx}))^2 \\ & - 4K_x(r - R + D_{x0} - r_{ccx})(2r - 2R)K_{R_y} && (3.4)\\ =& (K_{R_y}\theta_{y0} + K_x\epsilon''_{x0}(\mu r + \mu r_{ccx}))^2 - 4K_x\epsilon''_{x0}(2r - 2R)K_{R_y} && (3.5)\end{aligned}$$

ϵ''_{x0} will not depend on the value of r_{ccx}. Thus partial derivative of the discriminant:

$$\frac{\partial \Delta}{\partial r_{ccx}} = 2(K_{R_y}\theta_{y0} + \mu K_x\epsilon''_{x0}(r + r_{ccx}))\mu K_x\epsilon''_{x0} \quad (3.6)$$

The left side two point contact is happening with the initial condition of $\theta_{y0} > 0$ and $\epsilon_{x0} < 0$, so it can be expected that $\epsilon''_{x0} < 0$. And using the same assumption $K_{R_y}\theta_{y0} >> \mu K_x \epsilon''_{x0} r$ as earlier, the derivative will become:

$$\frac{\partial \Delta}{\partial r_{ccx}} = 2\mu K_x K_{R_y} \theta_{y0} \epsilon''_{x0} + 2(\mu K_x \epsilon''_{x0})^2 r_{ccx} \tag{3.7}$$

The first part is always negative and the second part is negative when $r_{ccx} < 0$. So Δ would get bigger as r_{ccx} moves from zero to negative, and for some cases of tight clearance ratio or big initial angle error setup that the previous Δ is already close to zero, this small change would bring the discriminant to be some positive value. In conclusion, for a peg that is originally to the left of the hole and tilted slightly clockwise, an off compliance center on the left side can cause the peg to encounter two point contact.

3.2.2 Jamming Diagram

Since the insert direction is expected to be exactly the same as ideal compliance center case, without any control strategy changes, that is still $T_x = R_y = 0$, the same forces and torques in equations 2.96 to 2.98 can be used. However, if r_{ccx} is some negative value, the top line, indicating two point contact for $\theta_y > 0$, in the jamming diagram, Figure 2.6, will be moved downwards. And for a tight clearance ratio, two point contact can happen at a shallow insertion depth, so the top line can be even below the horizontal axis when l is small. In such a case, a positive $\frac{M_y}{F_z}$ will always be positive no matter how much F_z can be increased by moving downwards, meaning the combination of force and torque will result a point outside the jamming parallelogram. Thus, an off compliance center on the left side can cause jamming during two point contact without any change in control strategy.

3.2.3 l-θ Plot

Figure 3.2 shows the l-θ plot for a peg-and-hole assembly process for various r_{ccx} while $r_{ccz} = 0$. For a initial condition of positive θ_{y0} and negative ϵ_{x0}, the blue to green curves show $\frac{r_{ccx}}{r}$ values from -2 to 2. The plot verifies that for such initial conditions, a negative r_{ccx} can lead to two point contact phase, the concave part in the plot. It is also obvious that the chamfer crossing l-θ relationship is much more sensitive to r_{ccx} value change than other contact states. Later, a r_{ccx} estimation strategy would be shown based on this behavior.

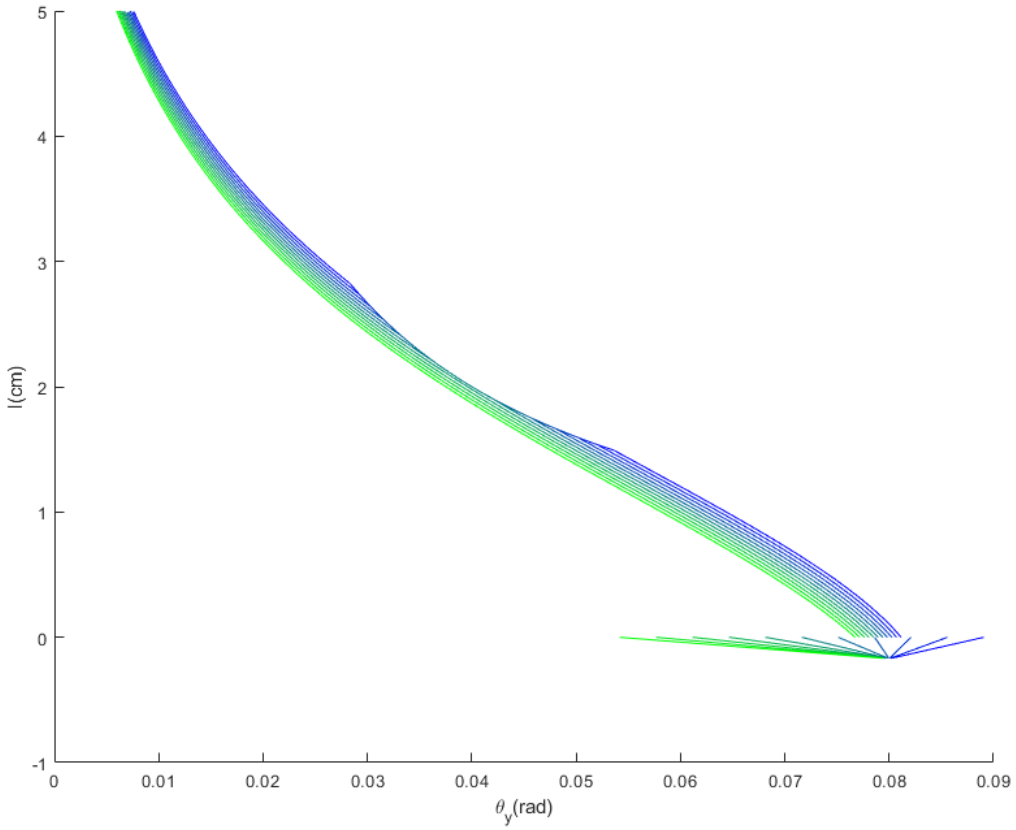

Figure 3.2. : l-θ Plot for Various r_{ccx}

3.2.4 Active Compliance

As for the equation 2.110 discussed for active compliance, the term for β is negative if $\mu < \cot\theta_y$, $\theta_y > 0$ and $\mu \geq 0$. So a negative r_{ccx} would increase $\frac{R}{r}$ and cause the curve to shift to the right, causing the jamming that was avoided to be possible to happen. Figure 3.3 shows how r_{ccx} affects the result when $r_{ccz} = 0$.

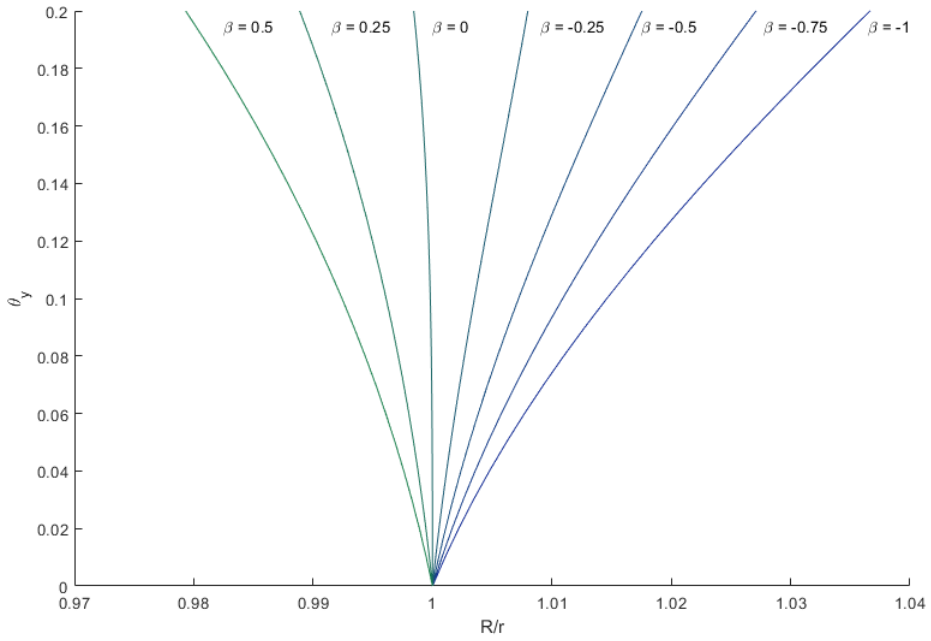

Figure 3.3. : Jamming Angle versus Radius Ratio when $\mu = 0.1$ for Various β

3.3 Force and Moment Plots

To have a better understanding of the effect an arbitrary compliance center has on the peg-and-hole problem, the forces and torques required to complete such an assembly process would be good indicators. The force and torque that sensors would detect for each contact states during the peg-and-hole assembly assuming a smooth quasi-static movement were mostly already discussed in the last chapter. The following

part will focus on the predicted force and torque versus insert depth assuming initial condition of $\theta_{y0} > 0$ and $\epsilon_{x0} < 0$ and no additional control input, as $T_x = R_y = 0$.

For the chamfer crossing contact state, equations 2.32 to 2.34 show how F_x, F_z and M_y would be functions of θ_y and s and equation 2.28 shows θ_y value depending on s. By using s values from s_0 to 0, the force and torque can be predicted. And when combined into plots of force and torque versus insert depth, a negative height difference between the peg tip and hole entrance, $-s\sin\alpha$, is used for virtual l.

During one point contact, equations 2.44 to 2.46 indicate how F_x, F_z and M_y are governed by θ_y and l and equation 2.42 shows the relationship between θ_y and l. By using l values from 0 to l_2 and from l_2' to insert depth that $\theta_y = 0$ or the depth that the peg is fully inserted, or in the cases of two point contact not happening from 0 all the way to these, the force and torque predicted versus insert depth can be drawn for one point contact.

And for the two point contact state, f_1 and f_2 would be too hard to decouple so F_x and M_y would be estimated by the position and the orientation of the peg and the passive compliance system. Here, the rotational difference between F_x and D_x is ignored for simplicity. From equations 2.25 and 2.7

$$F_x = K_x(D_x - D_{x0}) \tag{3.8}$$

$$M_y = K_{R_y}(\theta_y - \theta_{y0}) \tag{3.9}$$

The same geometry constraint during one point contact for D_x, equation 2.39, would still be valid for the left side being considered. So with two point contact geometry constraint shown in equation 2.48:

$$D_x = R - r + r_{ccx} + r_{ccz}\theta_y \tag{3.10}$$

So F_x would be:

$$F_x = K_x(r_{ccz}(\theta_y - \theta_{y0}) - \epsilon_{x0}'') \tag{3.11}$$

And since it is the force maintaining two point contact equilibrium being estimated, the relation from equation 2.72 should hold. So F_z can be predicted as:

$$F_z = \frac{M_y + (\mu r + r_{ccz} + \frac{l}{2})F_x}{r_{ccx} + \frac{l}{2\mu}} \tag{3.12}$$

$$= \frac{K_{R_y}(\theta_y - \theta_{y0}) + (\mu r + r_{ccz} + \frac{l}{2})K_x(r_{ccz}(\theta_y - \theta_{y0}) - \epsilon''_{x0})}{r_{ccx} + \frac{l}{2\mu}} \tag{3.13}$$

Thus F_x, F_z and M_y are functions of θ_y and l while $l\theta_y = 2R - 2r$. Using l values from l_2 to l'_2 can plot out the two point contact part.

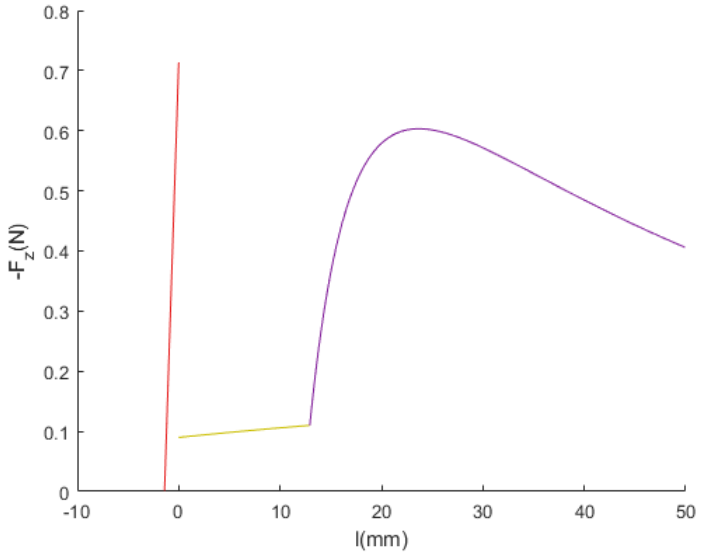

Figure 3.4. : F_z Prediction for a Passive Peg-and-hole Assembly

Figure 3.4 shows a general trend for the F_z required to smoothly insert the peg into the hole. Here note that F_z is the force sensor would read along the z_P axis, so the reaction forces from the hole would appear negative during the assembly process. The first straight line in red with negative insert depth is the chamfer crossing phase. The second part in yellow is one point contact and the last bit in purple is two point contact. It can also be seen that there is a huge force value jump between the end of the chamfer crossing and the start of one point contact. Such behavior could be

used to help identify which contact state the peg and the hole are in. And later this would be needed for r_{ccx} estimation.

For the off compliance center scenario, if two point contact can happen and r_{ccx} is some negative value for $\theta_{y0} > 0$, the denominator for F_z can be really small and thus make the F_z required to be extremely huge. The smallest l for two point contact would be l_2. For a nonzero r_{ccx}, equation 2.61 with no additional control becomes:

$$\theta_{y2} = \frac{K_{R_y}\theta_{y0} + (\mu r + \mu r_{ccx} + l_2 + r_{ccz})K_x(\epsilon''_{x0} + r_{ccz}\theta_{y0})}{(\mu r + \mu r_{ccx} + l_2 + r_{ccz})K_x r_{ccz} + K_{R_y}} \tag{3.14}$$

$r_{ccz} = 0$ and r_{ccx} should be roughly same magnitude as r. If l_2 is roughly the same magnitude of or even less than μr, with the previous assumption $K_{R_y}\theta_{y0} >> \mu K_x \epsilon''_{x0} r$, l_2 can be expressed as:

$$l_2 \cong \frac{2R - 2r}{\theta_{y0}} \tag{3.15}$$

So the denominator for F_z become:

$$r_{ccx} + \frac{l_2}{2\mu} = r_{ccx} + \frac{R - r}{\theta_{y0}\mu} \tag{3.16}$$

This means that a practically small clearance ratio, a relatively large initial angle error and a reasonable friction coefficient combining with a r_{ccx} that is roughly the same magnitude of r can lead to an infinitely large F_z. This case is the same as having the top line in the jamming diagram to be crossing the origin point.

3.4 Active Control

From all of the geometry and force analysis in the last chapter, it can be seen that the peg-and-hole assembly behavior can be affected by changing T_x and R_y. Equations 2.34, 2.46 and 2.72 show that the relationship between force and torque required for inserting is determined by position and orientation. Equations 2.32 and 2.44 show that the force and torque magnitude sensor would detect is determined by the current position of the peg, the position of the end factor and the compliance stiffness. And equations 2.28 and 2.42 have T_x and R_y terms implying the peg

orientation and position during the process could be indirectly controlled. But when T_x and R_y are variables depending on other variables, the analysis would need to be reviewed.

Here a control strategy of T_x and R_y is provided for pegs with the conditions of the off compliance center to behave like an ideal passive compliance device for the same initial rotational and transitional error relative to the hole. Suppose the control input T_x and R_y to be:

$$T_x = r_{ccz}(\theta_y - \theta_{y0}) \tag{3.17}$$

$$R_y = \frac{-r_{ccx}F_z + r_{ccz}F_x}{K_{R_y}} \tag{3.18}$$

Because T_x and R_y contain the variables depending on l and θ_y, the expressions cannot be plugged into the results directly. Now the same process for each contact states would be carried out again with the same move downwards motion for θ_{y0} and ϵ_{x0} to show the effect of such control input strategy.

For chamfer crossing, f_1 from equation 2.27 becomes:

$$f_1 = \frac{K_x}{\mathbf{B}}(r + r_{ccx} + r_{ccz}\theta_y - R - s\cos\alpha - \epsilon_{x0} - r_{ccx} - r_{ccz}\theta_{y0} - r_{ccz}(\theta_y - \theta_{y0})) \tag{3.19}$$

$$= -\frac{K_x}{\mathbf{B}}(\epsilon'_{x0} + s\cos\alpha) \tag{3.20}$$

So F_x and F_z would be:

$$F_x = -K_x(\epsilon'_{x0} + s\cos\alpha) \tag{3.21}$$

$$F_z = \frac{\mathbf{A}}{\mathbf{B}}K_x(s\cos\alpha + \epsilon'_{x0}) \tag{3.22}$$

Thus in this case M_y would be:

$$M_y = K_{R_y}(\theta_y - \theta_{y0} - R_y) \tag{3.23}$$

$$= K_{R_y}(\theta_y - \theta_{y0}) + r_{ccx}F_z - r_{ccz}F_x \tag{3.24}$$

$$= K_{R_y}(\theta_y - \theta_{y0}) - r_{ccx}f_1\mathbf{A} - r_{ccz}f_1\mathbf{B} \tag{3.25}$$

Combine with equation 2.24 and yield:

$$\theta_y = \frac{K_{R_y}\theta_{y0}\mathbf{B} + rK_x\mathbf{A}(\epsilon'_{x0} + s\cos\alpha)}{K_{R_y}\mathbf{B}} \tag{3.26}$$

Here the F_x, F_z and θ_y under such additional active control have the same result as equations 2.32, 2.33 and 2.28 with $T_x = R_y = 0$ and $r_{ccx} = r_{ccz} = 0$.

And for one point contact, f_1 from equation 2.41 becomes:

$$f_1 = K_x(l\theta_y + r - R + r_{ccx} + r_{ccz}\theta_y - \epsilon_{x0} - r_{ccx} - r_{ccz}\theta_{y0} - r_{ccz}(\theta_y - \theta_{y0})) \tag{3.27}$$

$$= K_x(l\theta_y - \epsilon'_{x0}) \tag{3.28}$$

So F_x and F_z in this case would be:

$$F_x = K_x(l\theta_y - \epsilon'_{x0}) \tag{3.29}$$

$$F_z = -\mu K_x(l\theta_y - \epsilon'_{x0}) \tag{3.30}$$

And then M_y would be:

$$M_y = K_{R_y}(\theta_y - \theta_{y0} - R_y) \tag{3.31}$$

$$= K_{R_y}(\theta_y - \theta_{y0}) + r_{ccx}F_z - r_{ccz}F_x \tag{3.32}$$

$$= K_{R_y}(\theta_y - \theta_{y0}) - \mu r_{ccx}f_1 - r_{ccz}f_1 \tag{3.33}$$

Combine it with equation 2.38:

$$\theta_y = \frac{K_{R_y}\theta_{y0} + (\mu r + l)K_x\epsilon'_{x0}}{(\mu r + l)K_x l + K_{R_y}} \tag{3.34}$$

Again F_x, F_z and θ_y are the same as previous analysis for one point contact with $T_x = R_y = 0$ and $r_{ccx} = r_{ccz} = 0$.

And for two point contact, the same geometry constraints are still valid. So putting equation 3.34 and 2.48 together gives:

$$\alpha l^2 + \beta l + \gamma = 0 \tag{3.35}$$

Here:

$$\alpha = K_x\epsilon''_{x0} \tag{3.36}$$

$$\beta = K_{R_y}\theta_{y0} + \mu K_x\epsilon''_{x0}r \tag{3.37}$$

$$\gamma = (2r - 2R)K_{R_y} \tag{3.38}$$

The solution l_2 and l_2' would be the same as the solution for equation 2.49 with $T_x = R_y = 0$ and $r_{ccx} = r_{ccz} = 0$.

And F_x for two point contact can be derived from equations 2.25, 2.39 and 2.48:

$$F_x = K_x(D_x - D_{x0} - T_x) \tag{3.39}$$

$$= K_x(l\theta_y + r - R + r_{ccx} + r_{ccz}\theta_y - \epsilon_{x0} - r_{ccx} - r_{ccz}\theta_{y0} - r_{ccz}(\theta_y - \theta_{y0})) \tag{3.40}$$

$$= - K_x\epsilon''_{x0} \tag{3.41}$$

With control R_y, M_y should be:

$$M_y = K_{R_y}(\theta_y - \theta_{y0} - R_y) \tag{3.42}$$

$$= K_{R_y}(\theta_y - \theta_{y0}) + r_{ccx}F_z - r_{ccz}F_x \tag{3.43}$$

Thus F_z to maintain equilibrium state, by using equation 2.72, would become:

$$F_z = \frac{K_{R_y}(\theta_y - \theta_{y0}) - (\mu r + \frac{l}{2})K_x\epsilon''_{x0}}{\frac{l}{2\mu}} \tag{3.44}$$

This result of F_x and F_z are the same as predicted in equation 3.13 assuming $r_{ccx} = r_{ccz} = 0$.

From all of the above, this active control strategy would make the peg go through the same θ_y and l relationships using the same F_x and F_z as an ideal RCC device. Only M_y is changed. Apparently, with the compliance center at a different location, it won't be possible to have the same M_y when forces and the relative position of the peg are the same. Referring to jamming diagram, left and right edge at $\pm\frac{1}{\mu}$ is fixed, while r_{ccx} only affects vertical axis intercept and r_{ccz} only affects slope. Thus only changing M_y value while keeping F_x and F_z untouched is possible to have the combination lie within the new parallelogram for the off compliance center.

This active control strategy does not rely on r_{ccz} being negligible. So if the off compliance center relative to the peg is known or is estimated by some means, integration of such active control and the passive compliance device can have any arbitrary compliance center to act like an ideal compliance center. So the advantage of a passive compliance device can be used on various peg-and-hole occasions.

For a unknown error compliance center in the peg gripped at an error angle case, the control strategy would be:

$$T_x = \hat{r}_{ccz}\Delta\theta_y \tag{3.45}$$

$$R_y = \frac{-\hat{r}_{ccx}F_z + \hat{r}_{ccz}F_x}{K_{R_y}} \tag{3.46}$$

Here $\hat{r}_{ccx}$ and $\hat{r}_{ccz}$ are the estimated off compliance center position relative to the peg tip, F_x and F_z are the values got from force and torque sensors and K_{R_y} is set as the experiential torsion stiffness about y axis of the compliance matrix. θ_y can be reflected by the readings from peg orientation minus an error while θ_{y0} would be the angle reading after visual servo aligns and before move downwards starts minus roughly the same error. Thus $\Delta\theta_y$, the rotational angle change sensed after peg alignment, should be able to represent $\theta_y - \theta_{y0}$ within the magnitude of sensor accuracy without knowing the actual orientation of the hole. The uncertainties were assumed to be mainly caused by vision and the errors from force torque sensors and angle sensors would be assumed to be much smaller. Although the T_x and R_y would only be carried out by changing the reference input of the robot position control, which means they at best would only have the accuracy of the actuators, the passive compliance device itself can help insertion even when the clearance is smaller than the robot accuracy. Thus such a control strategy, which does not rely on the information obtained from vision, where the dominant uncertainties come from, should help overcome the relatively large compliance center error.

3.5 r_{ccx} Estimation

From the previous l-θ plot part, it can be seen that r_{ccx} can affect the θ_y for chamfer crossing greatly. Now for a peg gripped at an error angle case, r_{ccz} is relatively small. So the eqaution 2.28 for chamfer crossing θ_y assuming $r_{ccz} = 0$ would be:

$$\theta_y = \theta_{y0} + \frac{K_{R_y}R_y\mathbf{B} - (r_{ccx} + r)\mathbf{A}K_x(-\epsilon'_{x0} - T_x - s\cos\alpha)}{K_{R_y}\mathbf{B}} \tag{3.47}$$

Rearrange and get r_{ccx} as:

$$r_{ccx} = -\frac{K_{R_y}\mathbf{B}(R_y + \theta_{y0} - \theta_y))}{K_x\mathbf{A}(\epsilon'_{x0} + T_x + s\cos\alpha)} - r \tag{3.48}$$

And equation 2.8 with small angle approximation indicates:

$$\epsilon_{x0} + T_x = r - R - s_0\cos\alpha \tag{3.49}$$

In other words, r_{ccx} can be estimated as:

$$\hat{r}_{ccx} = -\frac{K_{R_y}\mathbf{B}(R_y - (\theta_y - \theta_{y0}))}{K_x\mathbf{A}((s - s_0)\cos\alpha)} - r \tag{3.50}$$

$$= \frac{K_{R_y}(\sin\alpha - \mu\cos\alpha)\sin\alpha(R_y - \Delta\theta_y)}{K_x(\cos\alpha + \mu\sin\alpha)\cos\alpha\Delta z} - r \tag{3.51}$$

Here R_y is the control input, $\Delta\theta_y$ is the angle difference sensed from initial position, r and α are considered known values and K_{R_y}, K_x and μ are values gathered from previous experiments. Δz is the distance peg moved along the z_p axis since first contact with the chamfer. When there is first some reaction force sensed that exceeds the zero zones, a position reading along the peg z axis from the sensors would be recorded to represent $-s_0\sin\alpha$ minus some error. And any new position reading after that can be treated as $-s\sin\alpha$ minus roughly the same error. Thus this Δz reading can be used to estimate $-(s - s_0)\sin\alpha$ within the uncertainties of the robot position sensors without taking the hole position estimated by vision into account. Therefore such r_{ccx} estimation strategy would not be affected by the assumption that vision accuracy is poor.

For a complete peg-and-hole procedure, after vision moved the peg near the hole and the orientation of the hole was estimated, the peg will be inserted with a straight position control. The spike in F_z at the end of chamfer crossing would be used as an indicator to distinguish the contact states. The r_{ccx} estimation was run without any control input of T_x and R_y until the end of chamfer crossing. If the estimated r_{ccx} was large, the addition active control would be used for the rest of the peg-and-hole insertion to cancel out the majority effect of such off compliance center.

4. SIMULATION

Due to limitations on the access of experiment equipment, only simulations were done to verify the theoretical conclusions. Plots with realistic parameters were generated using MATLAB and simulation of peg-and-hole assembly problems were run with open source physics engine Project Chrono. The results shown would be able to prove the active control discussed in the last chapter is indeed necessary and helpful to the process.

4.1 MATLAB F_z Prediction

First two theoretical predictions of F_z would be shown to show how peg gripped at an error angle case could lead to jamming during two point contact. The parameters are selected as the following to be practical in real world cases. The radius of the peg is $r = 9.9$mm and the radius of the hole is $R = 10$mm. The friction coefficient between the peg and the hole for all contact states throughout the assembly is assumed to be $\mu = 0.1$. The stiffness of passive compliance device is chosen to be $K_x = 1$N/mm and $K_{R_y} = 10^4$N·mm/rad. These values represent the magnitude of actual RCC devices. It can be seen from previous analysis that if K_x, K_z and M_y are multiplied by the same amount, the peg behavior during insertion would not change as long as quasi-static motion is maintained. Only the magnitude of forces and torques being sensed would be different.

The clearance ratio selected is fairly large so the allowed vision uncertainty can be large enough for the following setups. Here the values chosen are specifically designed to lead to extreme results. The initial error after peg alignment would be $\theta_{y0} = 0.08$rad and $\epsilon_{x0} = -1.5$mm. And the off compliance center will be at $r_{ccx} = -13$mm and $r_{ccz} = -0.64$mm. This is equivalent to a 13cm long peg being

gripped with an error angle of 0.1rad or roughly 5.7 deg. This is also the same magnitude of uncertainty required for vision servo to avoid wedging.

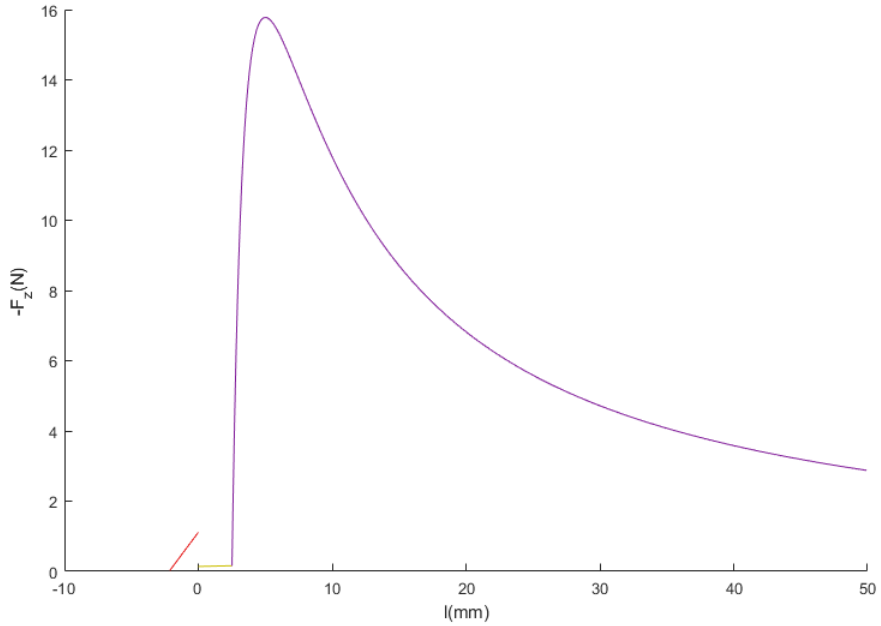

Figure 4.1. : F_z Prediction for the Ideal Compliance Center

Figure 4.1 shows the F_z required for the peg to be inserted quasi-statically with an ideal compliance center at the middle of the tip of the peg. Here the force is already quite large during the two point contact phase because the initial angle error θ_{y0} is relatively large. But the exact values would be largely depending on the stiffness of the passive device selected.

Figure 4.2 plots out the theoretical F_z required for the peg while $r_{ccx} = -0.013$ and $r_{ccz} = -0.00064$. The denominator $r_{ccx} + \frac{l_2}{2\mu}$ is so small that F_z has reached an extremely high value. And no matter what the actual stiffness value would be, these two plots have shown how a negative r_{ccx} with positive θ_{y0} and negative ϵ_{x0} initial condition can lead to potential failure.

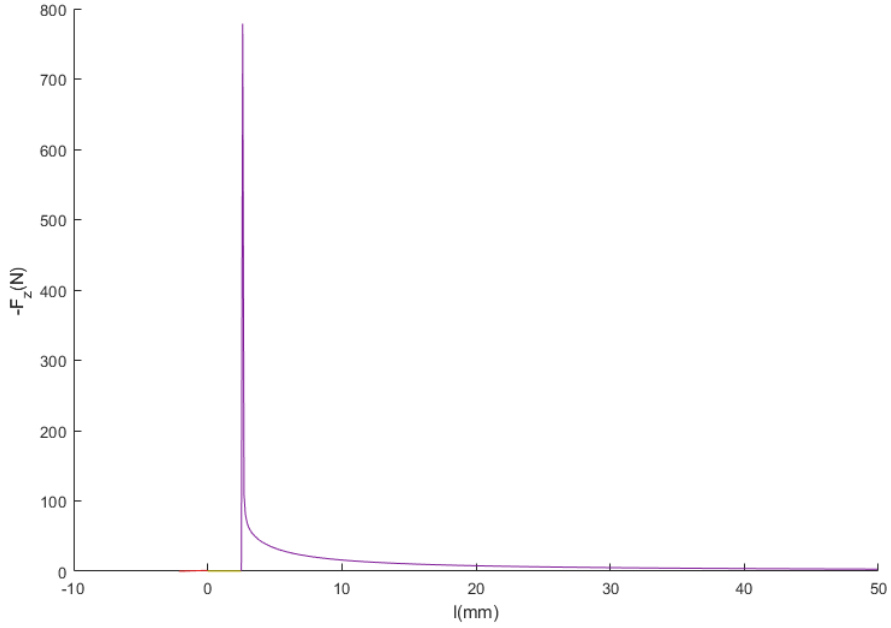

Figure 4.2. : F_z Prediction for the Off Compliance Center

4.2 Project Chrono Simulations

Additional simulations using $c++$ and open source physics engine Project Chrono were done to better verify the previous results. A screen capture is shown in Figure 4.3. The red shape is a set of triangle mesh to represent the hole. The blue cylinder is the peg and the little white ball represents the robot end factor. A marker fixed on the peg that is at the same location of the white ball will be the compliance center. The marker is connected to the white ball through two springs and a torsion spring. The effect of gravity is canceled out and the white ball will simply move downwards. Since no damping was set for the springs, to achieve better stability and mimic a quasi-static movement, the actual forces and moments applied in the physics engine simulation is set to be a-hundredth of supposed values to not cause apparent acceleration. But the values used for later plot generation are restored back to the

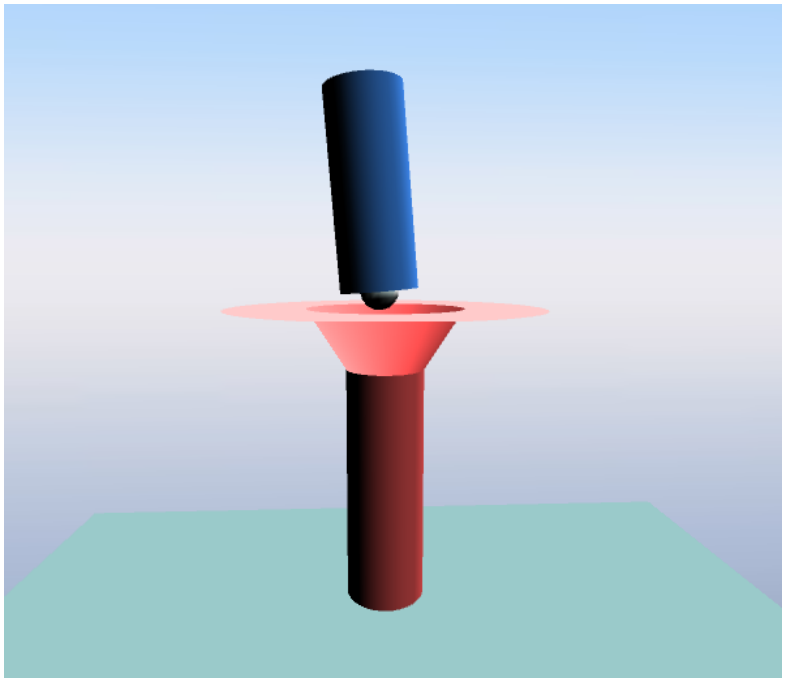

Figure 4.3. : Project Chrono Simulation

same K_x and K_{R_y} as above. As discussed earlier, such change would not affect the insertion depth and rotation relationship according to theoretical analysis.

4.2.1 Ideal Compliance Center

Figure 4.4 to 4.7 shows the physics engine simulation result along with the theoretical MATLAB predictions for a ideal compliance center $r_{ccz} = r_{ccx} = 0$. Here the forces and moments for a small clearance ratio will lead to unavoidable small oscillation. For the l-θ plot, the maximum and minimum θ_y is displaced. It is obvious that the peg will be more stable at latter part of two point contact states. It can also be noticed that there is a small increase of insertion depth at the start of two point contact phase for all plots. This is because negative contact distance can happen for the physics engine simulation, which means that the hole edge has penetrated into the peg and the peg tip has penetrated the other side of the hole a little bit for the

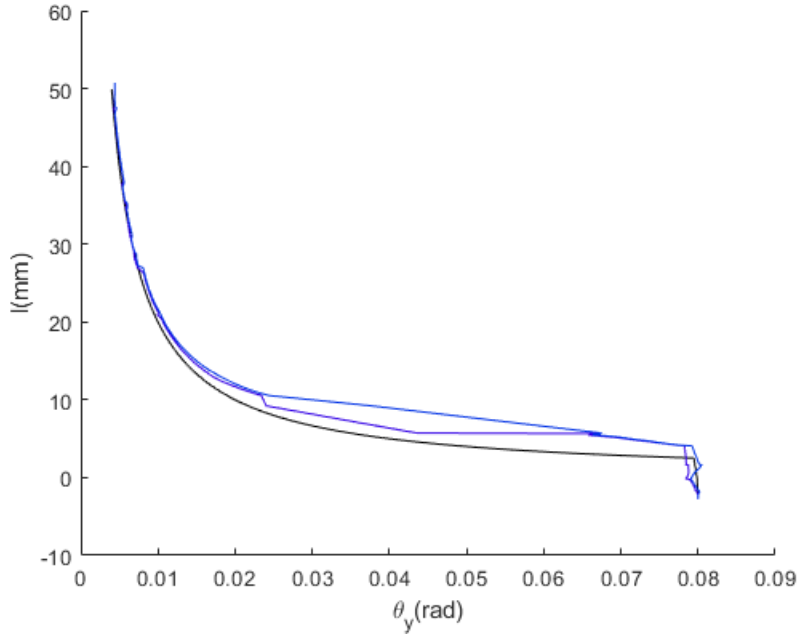

Figure 4.4. : Simulation l-θ for the Ideal Compliance Center

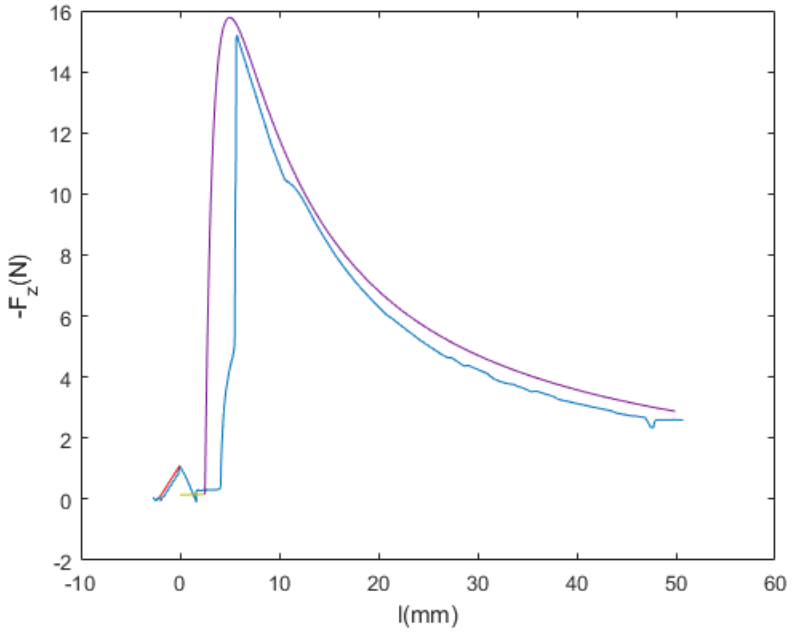

Figure 4.5. : Simulation F_z for the Ideal Compliance Center

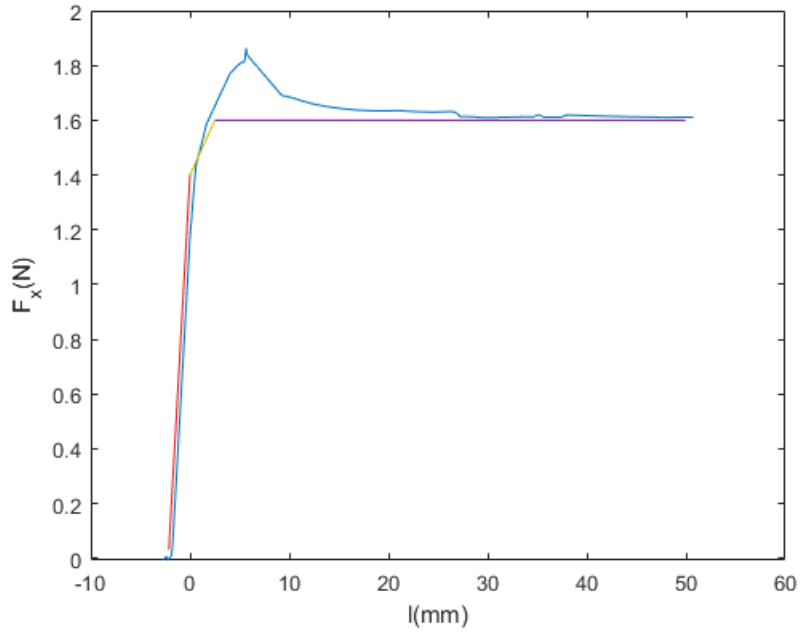

Figure 4.6. : Simulation F_x for the Ideal Compliance Center

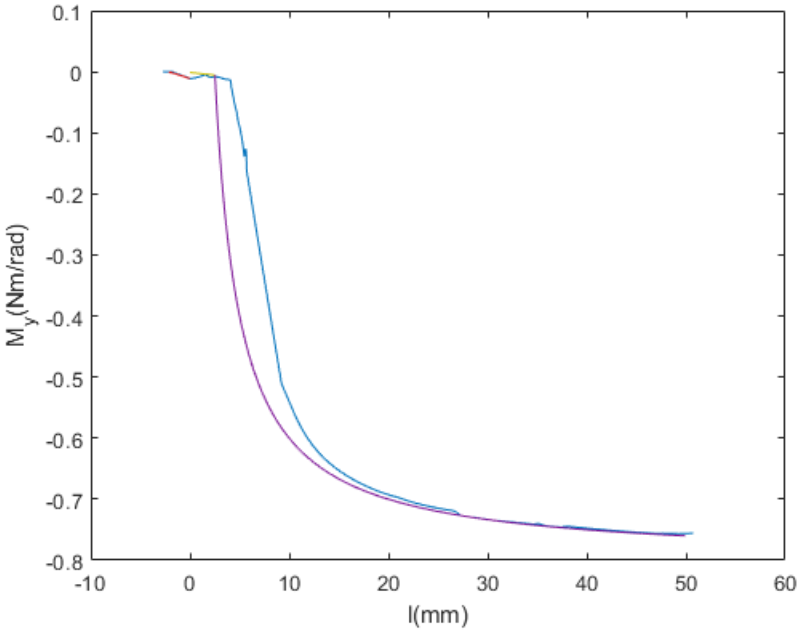

Figure 4.7. : Simulation M_y for the Ideal Compliance Center

reaction forces to achieve balance. But the overall trend has shown such simulation fits the theoretical predictions pretty well.

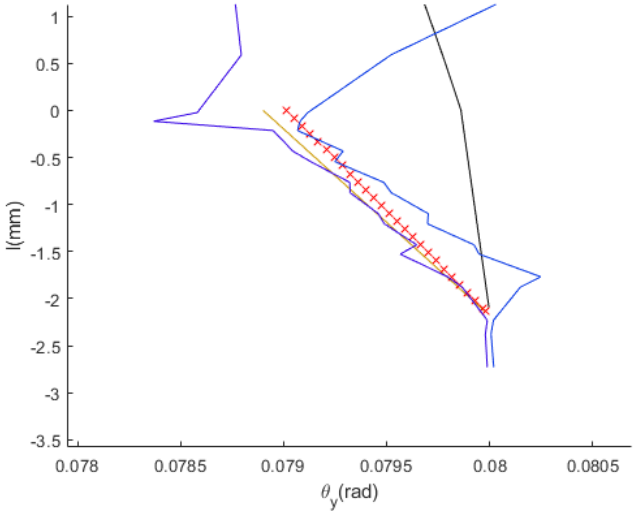

Figure 4.8. : Simulation versus Theory for Chamfer Crossing

Also figure 4.8 provides a detailed look at the chamfer crossing behavior for the ideal compliance center case. The yellow line is the linear approximation using equation 2.28 and the red crosses are the θ_y results from numerically solving the equation 2.20. This helps show that the approximations are reasonable and the θ_y value jump for l-θ plot also fits the actual peg behavior.

4.2.2 Off Compliance Center

Figure 4.9 and 4.10 show the Project Chrono simulation result for peg gripped at an error angle case. The insertion is jammed at a shallow depth and the peg stops moving even while the amount of F_z keeps getting bigger. Even after the F_z has exceeded the prediction values of F_z at a larger insertion depth l, the jamming is still there. This is probably due to the negative contact distance stated above. Under such large forces, the peg might be constantly overlapping the hole edge, leading the actual insertion depth inside the hole to be smaller than it appears. Also the chamfer

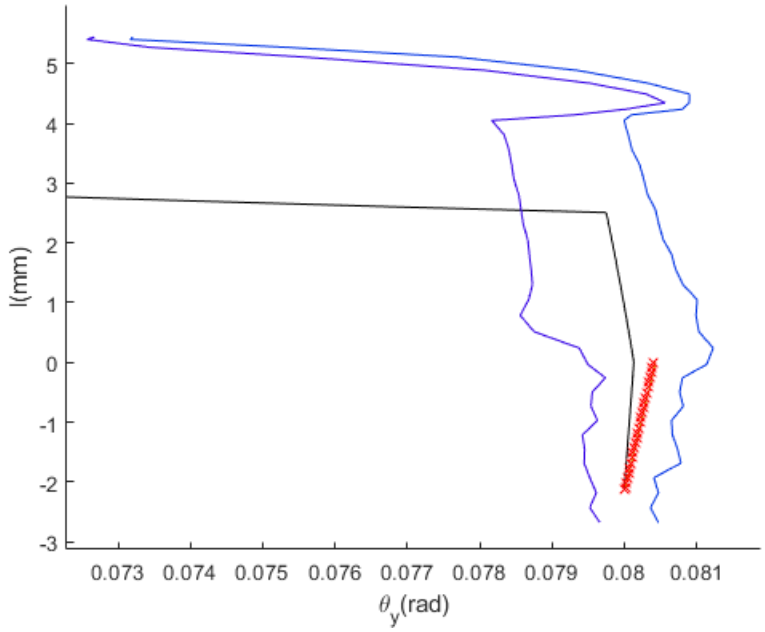

Figure 4.9. : Simulation l-θ for the Off Compliance Center

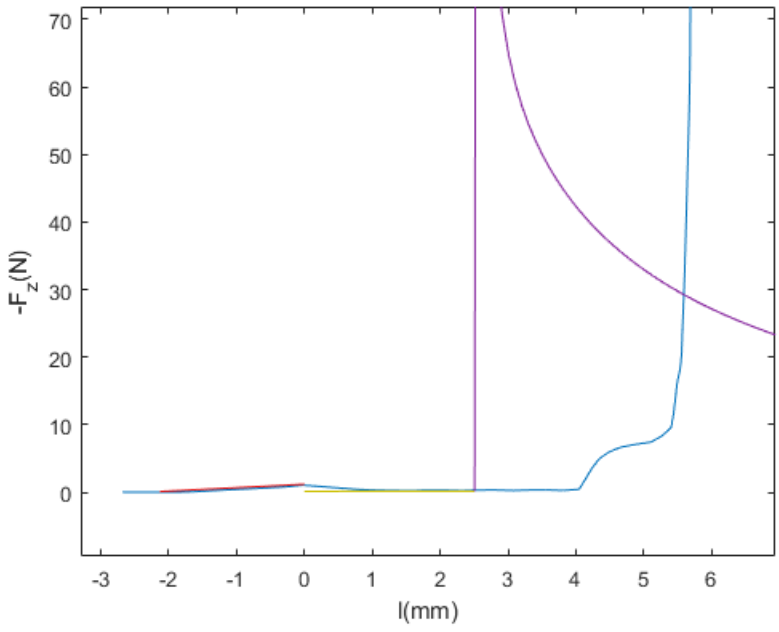

Figure 4.10. : Simulation F_z for the Off Compliance Center

crossing behavior is shown in the l-θ plot as well. And this will be used to estimate r_{ccx}.

4.2.3 Integration of Active Control and Passive Compliance

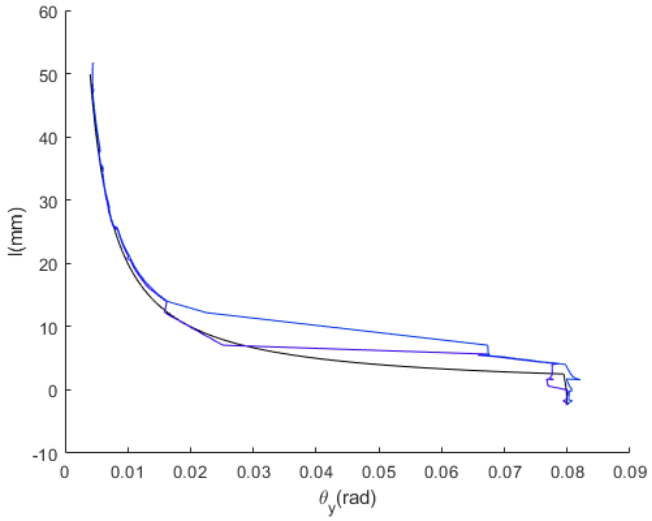

Figure 4.11. : Active Control Simulation l-θ Plot

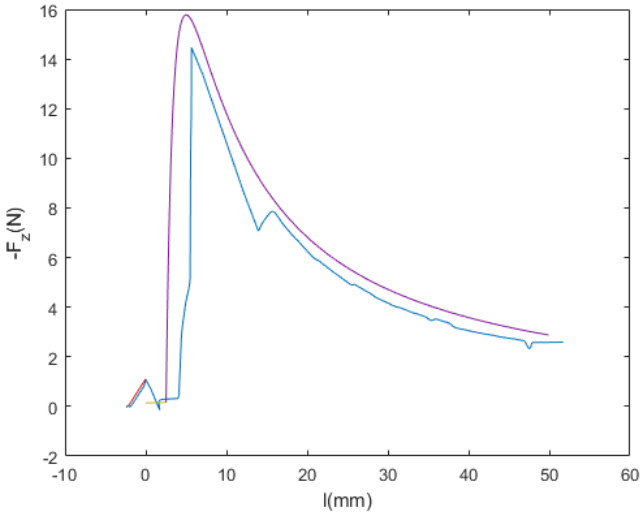

Figure 4.12. : Active Control Simulation F_z Plot

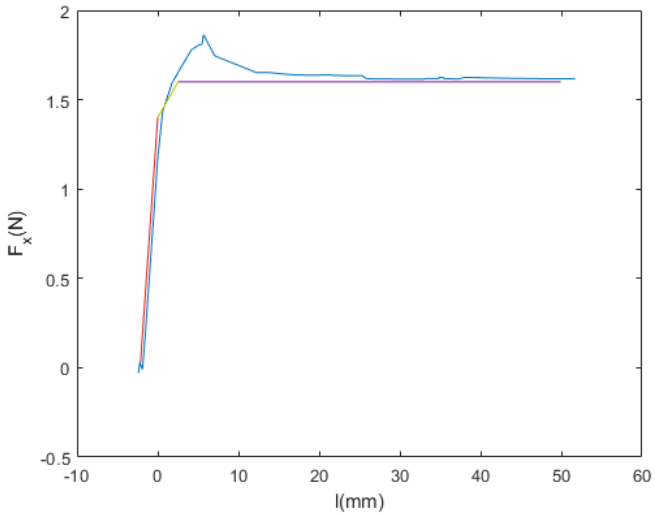

Figure 4.13. : Active Control Simulation F_x Plot

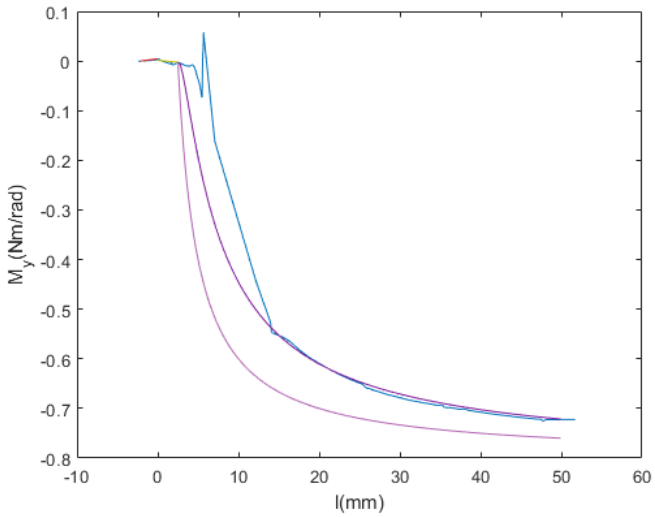

Figure 4.14. : Active Control Simulation M_y Plot

Figure 4.11 to 4.14 are the results from combination active control and passive compliance. Here r_{ccz} is assumed to be negligible and the control input of $T_x = 0$ and $R_y = 0.013F_z/K_{R_y}$ after chamfer crossing state is used. It can be seen that the l-θ, F_z and F_x for the off compliance center would be almost the same as the ideal

compliance center case. The major difference is a little acceleration along the z axis after the spike of F_z. And in the last M_y plot, a lighter purple curve showing the M_y for the ideal case is also provided together with the darker purple one for the theoretical prediction with this active control. These results show the effect of the combination of active control with passive compliance. Therefore, with a relatively small r_{ccx} and r_{ccz} error, since the θ_y, F_x and F_z would behave like the ideal with additional active control, the new M_y would also be within a reasonable range and potential jamming caused by the off compliance center can be avoided.

4.2.4 Active control with Estimated r_{ccx}

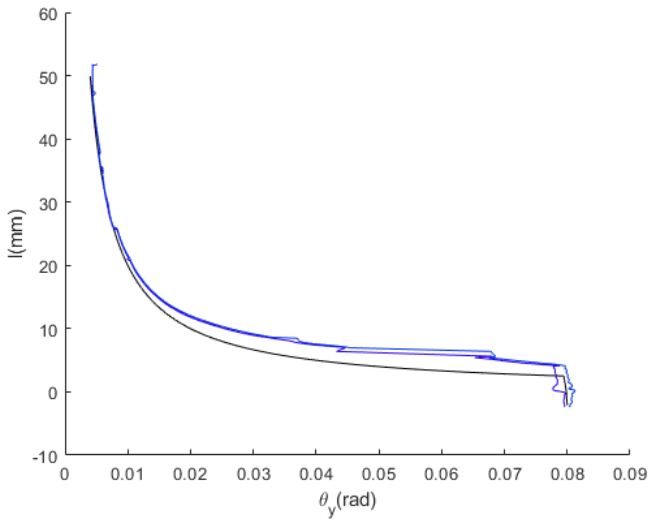

Figure 4.15. : Active Control Simulation l-θ with $\hat{r}_{ccx} = -0.0105$

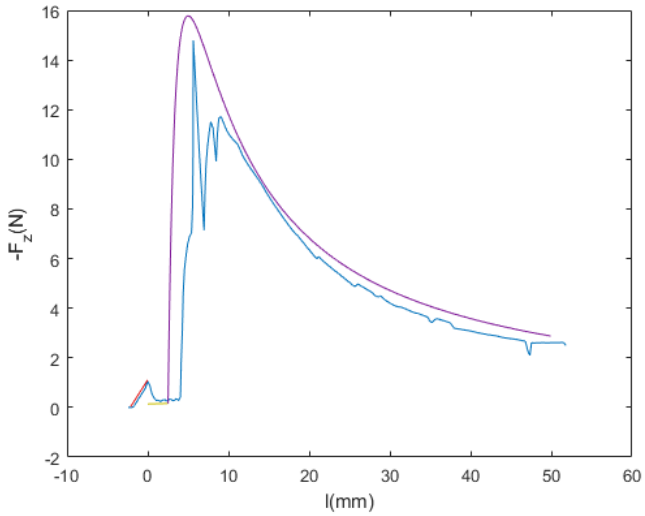

Figure 4.16. : Active Control Simulation F_z with $\hat{r}_{ccx} = -0.0105$

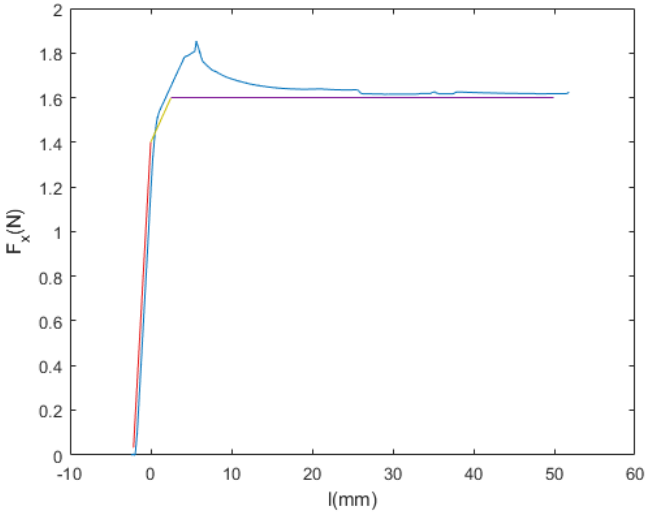

Figure 4.17. : Active Control Simulation F_x with $\hat{r}_{ccx} = -0.0105$

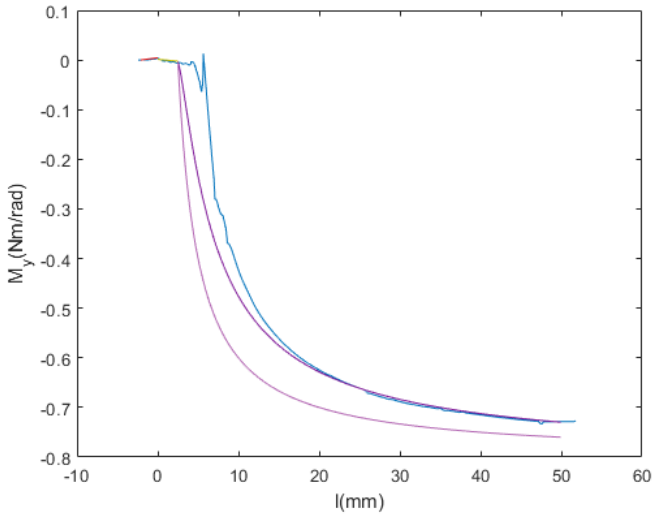

Figure 4.18. : Active Control Simulation M_y with $\hat{r}_{ccx} = -0.0105$

Finally $\hat{r}_{ccx}$ is combined with the active control. From various trials, it is found that the estimation is most accurate around the place when F_z is peaked around chamfer crossing. It is probably due to the magnitude of the variables are relatively larger compared to the change caused by oscillations. So with $T_x = 0$ and $R_y = 0$ during the chamfer crossing until F_z drastically changed. The equation 3.51 is used to get a result of $\hat{r}_{ccx} \approx -0.0105$. Then additional control of $T_x = 0$ and $R_y = 0.0105F_z/K_{R_y}$ is applied until the end. From figures 4.15 to 4.18, it can be seen that, although the F_z values are less stable, the potential jamming is still avoided even when $\hat{r}_{ccx}$ does not exactly match r_{ccx}.

5. SUMMARY

This thesis did the analysis of the peg-and-hole problem for arbitrary compliance centers and proved an active control strategy that can cancel out most of the problems caused by the compliance center not being at the tip of the peg. The peg gripped at an error angle case has proven to be able to cause jamming in certain scenarios and the estimation for the compliance center for such cases is shown to be useful with the active control. This setup is meaningful because it should be able to utilize the advantages of passive compliance devices most of the time and the additional active control can help deal with cases when error is large without the need to stop and re-grip. Also the arbitrary compliance center model with the integration of active control and passive compliance can be further used in other real life cases such as a fixed RCC with various different size pegs. As long as the dimensions of the peg and the compliance center relative to the tip of the peg can be estimated, the active control and passive compliance can even insert the peg into a hole with the clearance smaller than the robot accuracy.

6. RECOMMENDATIONS

In the problem chapter, it was discussed how some off compliance centers can hinder the assembly process for certain initial conditions. However, it is also implied that some other off compliance center can help avoid two point contact jamming for these initial conditions. So if the signs of the initial errors can be controlled by the approach and alignment strategy, then varying the compliance center to be off in some way can be beneficial to the peg-and-hole problem.

For future research work, here are some recommended aspects to look into. This thesis has assumed r_{ccz} of the off compliance center to be small. However, for an unknown compliance center, a better compliance center location estimation algorithm would be needed to find both $\hat{r}_{ccx}$ and $\hat{r}_{ccz}$. This thesis has also assumed a limited degree of freedom in the 2-D scenario at the start, how an arbitrary compliance center would affect the peg-and-hole problem in 3-D and what active control should look like for 3-D still require further studies for more real world applications.

REFERENCES

REFERENCES

[1] Paul C Watson. Remote center compliance system, July 4 1978. US Patent 4,098,001.

[2] Daniel E Whitney et al. Quasi-static assembly of compliantly supported rigid parts. *Journal of Dynamic Systems, Measurement, and Control*, 104(1):65–77, 1982.

[3] Namik Ciblak and Harvey Lipkin. Design and analysis of remote center of compliance structures. *Journal of robotic systems*, 20(8):415–427, 2003.

[4] RH Sturges Jr and S Laowattana. Design of an orthogonal compliance for polygonal peg insertion. 1996.

[5] Jing Xu, Zhimin Hou, Zhi Liu, and Hong Qiao. Compare contact model-based control and contact model-free learning: A survey of robotic peg-in-hole assembly strategies. *arXiv preprint arXiv:1904.05240*, 2019.

[6] T Yamashita, I Godler, Y Takahashi, K Wada, and R Katoh. Peg-and-hole task by robot with force sensor: Simulation and experiment. In *Proceedings IECON'91: 1991 International Conference on Industrial Electronics, Control and Instrumentation*, pages 980–985. IEEE, 1991.

[7] Kuangen Zhang, MinHui Shi, Jing Xu, Feng Liu, and Ken Chen. Force control for a rigid dual peg-in-hole assembly. *Assembly Automation*, 2017.

[8] Tadanobu Inoue, Giovanni De Magistris, Asim Munawar, Tsuyoshi Yokoya, and Ryuki Tachibana. Deep reinforcement learning for high precision assembly tasks. In *2017 IEEE/RSJ International Conference on Intelligent Robots and Systems (IROS)*, pages 819–825. IEEE, 2017.

[9] Fengming Li, Qi Jiang, Yibin Li, Meng Wei, and Rui Song. Modeling contact state of industrial robotic assembly using support vector regression. In *2018 IEEE 8th Annual International Conference on CYBER Technology in Automation, Control, and Intelligent Systems (CYBER)*, pages 646–651. IEEE, 2018.

[10] Ibrahim F Jasim and Peter W Plapper. Contact-state monitoring of force-guided robotic assembly tasks using expectation maximization-based gaussian mixtures models. *The international journal of advanced manufacturing technology*, 73(5-8):623–633, 2014.

[11] Siddharth R Chhatpar and Michael S Branicky. Search strategies for peg-in-hole assemblies with position uncertainty. In *Proceedings 2001 IEEE/RSJ International Conference on Intelligent Robots and Systems. Expanding the Societal Role of Robotics in the the Next Millennium (Cat. No. 01CH37180)*, volume 3, pages 1465–1470. IEEE, 2001.

[12] Te Tang, Hsien-Chung Lin, Yu Zhao, Wenjie Chen, and Masayoshi Tomizuka. Autonomous alignment of peg and hole by force/torque measurement for robotic assembly. In *2016 IEEE international conference on automation science and engineering (CASE)*, pages 162–167. IEEE, 2016.

[13] Wei Wang, Robert NK Loh, and Edward Y Gu. Passive compliance versus active compliance in robot-based automated assembly systems. *Industrial Robot: An International Journal*, 1998.

[14] Sangcheol Lee. Development of a new variable remote center compliance (vrcc) with modified elastomer shear pad (esp) for robot assembly. *IEEE Transactions on Automation Science and Engineering*, 2(2):193–197, 2005.

[15] Hee-Chan Song, Young-Loul Kim, and Jae-Bok Song. Automated guidance of peg-in-hole assembly tasks for complex-shaped parts. In *2014 IEEE/RSJ International Conference on Intelligent Robots and Systems*, pages 4517–4522. IEEE, 2014.

[16] Mohamad Bdiwi, Jozef Suchỳ, Michael Jockesch, and Alexander Winkler. Improved peg-in-hole (5-pin plug) task: Intended for charging electric vehicles by robot system automatically. In *2015 IEEE 12th International Multi-Conference on Systems, Signals & Devices (SSD15)*, pages 1–5. IEEE, 2015.

[17] W Haskiya, K Maycock, and J Knight. Robotic assembly: chamferless peg-hole assembly. *Robotica*, 17(6):621–634, 1999.

[18] Sergio Simunovic. Force information in assembly processes. In *5th International Symposium on Industrial Robots*, pages 415–431, 1975.

[19] Seth Hutchinson, Gregory D Hager, and Peter I Corke. A tutorial on visual servo control. *IEEE transactions on robotics and automation*, 12(5):651–670, 1996.